UNIVERSITY OF BERGEN

Geophysical Institute

MASTER THESIS IN PHYSICAL OCEANOGRAPHY

Oil Spill Modeling in Sea Ice Covered Ocean

Author: Victor Cesar Martins de Aguiar

Supervisor: Dr. Lars Robert Hole

Co-supervisor: Dr. Knut Barthel

June 1, 2021

"The Earth is the only world known so far to harbor life. There is nowhere else, at least in the near future, to which our species could migrate. Visit, yes. Settle, not yet. Like it or not, for the moment the Earth is where we make our stand."

Carl Sagan, Pale Blue Dot, 1994

Abstract

The ongoing reduction in extent and thickness of sea ice in the Arctic allows the expansion of shipping activity and oil exploration in the high north, and with that a potential increased risk of oil spill in ice covered areas. This thesis asses the response of two oil-in-ice surface drift models implemented in an open-source Lagrangian framework and forced by four different ice-ocean products (RIOPS, TOPAZ4 real-time forecast system, TOPAZ4 reanalysis and SVIM). Both approaches were evaluated over three sets of simulations: (I) a field experiment conducted in the Barents Sea marginal ice zone in 2009; (II) observed trajectories of buoys in the ice pack and in the Barents Sea marginal ice zone; and (III) stochastic simulations (960 runs, from 1998 to 2017) to reproduce a hypothetical oil spill in the Kara Sea. Results from experiments (I) and (II) indicate that the two drift models provide similar response both in the ice pack and the marginal ice zone under the same forcing. It was also found that finer horizontal resolution ice-ocean products (RIOPS and SVIM) did not reproduce better the observed drifts. The experiment (III) revealed that the sea ice concentration (%) field dictates the spread, the predominant direction of trajectories and the distance (km) traveled by the cloud of particles (SVIM: -1.41 km/% and TOPAZ4 reanalysis: -1.24 km/%).

Acknowledgments

I would like to thank my supervisor, Dr. Lars Robert Hole, for the great guidance and friendship we have been sharing over these two last years. Thank you for trusting on my capacity and providing so many resources that helped me to come and continue studying in Bergen. My special thanks to my co-supervisor Prof. Dr. Knut Barthel for guiding me over the development of this work and through the fantastic world of numerical modeling. Your lectures and organization inspire me.

I also dedicate this work to my friends and co-workers from MET, in special Knut-Frode Dagestad, Gaute Hope, Patrik Bohlinger, Øyvind Breivik and Birgitte Furevik for the scientific discussions, adventures and for including me in the group. In addition, I would like to thank Dr. Graig Sutherland (Environment and Climate Change Canada), Dr. Jean Rabault (MET - Oslo), Dr. Alexei Bambulyak (Akvaplan-niva AS), Dr. Magnus Aune (Akvaplan-niva AS) and Dr. Denis Moiseev (Murmansk Marine Biological Institute) for the valuable discussions.

The COVID-19 pandemic days highlighted how friendships and human contact are indispensable for my mental health and were key points to overcome such a dark period. I thank, from the bottom of my heart, my friends Martin Pečnjak, Ole Rieke, Joan Mateu Horrach Pou, Astrid Myren, Torunn Sandven Sagen and Leilane Gonçalves dos Passos for all the moments we shared together.

To my beloved family and friends in Brazil, that supported and embraced me despite the long distance. To Mari Vanharanta, that has followed my journey and supported me since 2017. Todo meu amor à vocês!

Lastly, I thank the The Nansen Legacy project (Arven etter Nansen) and the Fram Centre, through the MIKON / OSMICO project, for the funding provided to conduct this thesis. Without this indispensable financial support, my studies and this work would not have been possible to be accomplished. Lastly, I acknowledge Dr. Tor Nordam (SINTEF Ocean) for sharing the FEX09 data with me, and Dr. Wendy Ermold (University of Washington) and Dr. Jennifer Hutchings (Oregon State University) for the valuable discussion and guiding regarding the IABP data.

Fram Centre

Contents

List of Figures

List of Tables

List of abbreviations

AeN Arven etter Nansen

AMSR-2 Advanced Microwave Scanning Radiometer 2

CESM-LE Community Earth System Model Large Ensemble project

CICE Los Alamos Sea Ice Model

CMEMS ARC-MFC Arctic – Monitoring Forecasting Centre of the Copernicus Marine Environment Monitoring Service

DAMSA Danish Maritime Safety Administration

DMI Danish Meteorological Institute

EB Elasto-Brittle sea ice rheology

ECCC Environment and Climate Change Canada

ECMWF European Centre for Medium-Range Weather Forecasts

EnKF Ensemble Kalman Filter

EUMETSAT European Organisation for the Exploitation of Meteorological Satellites

EVP Elastic-Viscous-Plastic sea ice rheology

FEX09 Field EXperiment conducted in the Barents Sea in 2009

GDPS Global Deterministic Prediction System

GIOPS Global Ice and Ocean Prediction System

HARMONIE-AROME HIRLAM-ALADIN Research on Mesoscale Operational Numerical Weather Prediction in Euromed — Application of Research to Operations at Mesoscale

IABP International Arctic Buoy Program

JIP Joint Industry Program

MC Murmansk Current

MCC Murmansk Coastal Current

MET Norwegian Meteorological Institute

MICOM Miami Isopycnic Coordinate Ocean Model

MIZ Marginal Ice Zone

NAC Norwegian Atlantic Current

NCC Norwegian Coastal Current

NEMO Nucleus for European Modelling of the Ocean

NERSC Nansen Environmental and Remote Sensing Center

neXtSIM neXt generation Sea Ice Model

NORA3 NOrwegian ReAnalysis 3 km

NPD Norwegian Petroleum Directorate

NSIDC National Snow and Ice Data Center

NSR Northern Sea Route

NtCC North Cape Current

OILMAP OIL and Spill Impact MAPping

OSCAR Oil Spill Contingency And Response

OSI-SAF Ocean and Sea Ice Satellite Application Facility

RIOPS Regional Ice and Ocean Prediction System

ROMS Regional Ocean Modeling System

Scm oe Standard cubic metres of oil equivalent

SIMAP Spill Impact Model Application

SIZEX Seasonal Ice Zone Experiment

SODA Simple Ocean Data Assimilation

SMHI Swedish Meteorological and Hydrological Institute

TOPAZ Towards an Operational Prediction system for the North Atlantic European coastal Zones

WFF Wild World Foundation

YOPP Year of Polar Prediction

Chapter 1

Introduction

1.0.1 Background

Oil spill releases in the marine environment have been observed since the beginning of the XX century and arose as major problem in the 1960s as a result of the development of supertanker ships, offshore installations and oil exploration over continental shelves Carpenter (2019). Since then, major accidents (*e.g. Amoco Cadiz*, France - 1978; *Deepwater Horizon*, USA - 2010) have released massive amounts of oil in the ocean, directly impacting fish stocks, bird colonies and human resources. The OSPAR Convention (Convention for the Protection of the Marine Environment of the North-East Atlantic) reported that more than 1350 offshore operational installations were present in the maritime zone under their jurisdiction (OSPAR Commission, 2021). The same commission reported that 4119 tonnes of oil were discharged and spilled in the North Sea in 2017, being Norway responsible for about 40 % of that (Commission, 2017, Table 5e).

In addition to the current operations, it is estimated that over 7800 sunken ships during the World War II lay on the seafloor, 124 of them in the Arctic (Monfils, 2005). This potential risk of oil pollution in ice covered waters comes on the top of a crescent shipping activity and interest on oil resources in the polar region. Even though the number of confirmed oil slicks and large oil spills (> 700 tonnes) have decreased over the years (Carpenter, 2019; The International Tanker Owners Pollution Federation, 2020), the risks associated to oil exploration and transportation are inherent and as such, research efforts have been made to improve our knowledge about the processes involved on the weathering and transport of oil in the ocean. Large oil-in-ice studies started by the middle of the 1970s with the Canadian Government Beaufort Project (Wilkinson et al., 2017) and a series of laboratory and field experiments have been conducted conducted since then (e.g. The Joint Industry Programme Sørstrøm et al., 2010).

When oil gets in contact with the environment it undergoes on a series of processes known as transport and weathering and these are essentially the same whether in the presence of sea ice or not (Afenyo et al., 2016). The first encompasses a range of processes (*e.g.* advection, spreading, dispersion and sedimentation) that transport oil from one place to another, both at the sea surface and in the water column (Afenyo et al., 2016).

In general terms, oil advection ($\mathbf{v}_{oil}$), also known as oil drift, is characterised by the displacement of the oil slick by the ocean currents ($\mathbf{v}_{water}$) and a fraction (f) of the wind speed ($\mathbf{v}_{wind}$) as:

$$\mathbf{v}_{oil} = \mathbf{v}_{water} + (f \times \mathbf{v}_{wind}) \tag{1.1}$$

Another major transport process that increases the surface area of an oil slick in the subsequent hours after the spill is to so-called spreading. In calm waters, and considering that the pour point is lower than the ambient temperature, an oil slick would spread in a circular shape as time evolves, with its thickness diminishing as the surface area increases until it reaches a minimum value of 10^{-2} to 10^{-3} cm, when it gets naturally dispersed. Spreading is classically described as a sequence of three different balance of forces that acts upon the slick over time in the following order: gravity-inertia, gravity-viscous and surface tension-viscous (Fay, 1969). In the presence of sea ice, spreading is generally reduced due to the presence of the ice floes and the oil thickness might not reach the minimum value as in open waters (Afenyo et al., 2016). Moreover, since the oil can be located on the top and under the floes, its spreading is also dependent on the surface and bottom roughness and this can be seen as a limiting factor in oil-in-ice modeling since this type of information is hardly provided by ice models. Thorough reviews regarding the topic can be found in Yapa and Dasanayaka (2006); Afenyo et al. (2016).

The third main transport process is natural dispersion and it happens when the oil slick is fragmented into oil droplets. Natural dispersion is intimately related to the sea state, *i.e.*, oil slicks are more easily dispersed into droplets where the sea surface turbulence is more intense, and to the oil slick properties itself. In other words, the density and viscosity of the spilled oil also play a key role on the susceptibility of dispersion: viscous, crude oils such as Bunker C are not easily dispersed as the refined products. Moreover, since oils are inherently weathered when in contact with the environment, timing is also crucial.

Dispersion, caused mainly by wave breaking, is also responsible for promoting the entrainment of oil droplets into the water column. There, particles are subject to vertical motions with the possibility of droplets resurfacing and coalescing back within the slick. As presented thoroughly in Subsection 2.1.2, but anticipated here, the droplet diameter (d) dictates how

fast particles can float back to the sea surface, and larger droplets ($d \geq 50\mu$m) will not stay in the water column for more than a few seconds (Fingas, 2014).

Dispersion of oil slicks, either by natural causes or enhanced by dispersants, increases the surface area on which marine bacteria and other organisms may colonize and biodegrade the oil (Das and Chandran, 2011). Biodegradation, differently from the others described above, is not a transport, but a weathering process. The latter plays a significant role on the alteration of physicochemical properties of the oil, changing its viscosity, density, water content, rheology and toxicity, for example (Fingas, 2012). Biodegradation, nor any of the weathering processes, is variable in time and its ability to degrade oil depends on the environmental conditions as well as on the oil chemical properties.

Transport and weathering processes, as those described above, are essentially the same worldwide, including in cold, ice covered waters. However, since temperature is a key factor, oil spilled in high latitude regions might behave differently than in tropical areas. For instance, evaporation and biodegradation rates may decrease significantly in low temperatures (Afenyo et al., 2016), and depending on the oil chemical properties, the oil might even solidify and stop spreading. There are also processes exclusive to regions where sea ice is present, such as encapsulation, percolation through brine channels, being stuck in ice keels and ridges or resurfacing into leads (Afenyo et al., 2016). Furthermore, the ice cover dampens wave activities, thus decreasing dispersion, entrainment and emulsification (Brandvik et al., 2009). In addition, if encapsulated, oil can remain unweathered, thus preserving its toxic properties, travel long distances and potentially impact areas initially unharmed (Wilkinson et al., 2017).

The knowledge of the oil type, spill location and its drift and fate are key factors considered by decision makers on response countermeasures. The main objective in any mitigation plan is to retrieve the maximum amount of the oil from the environment impacting it as little as possible (Taylor et al., 2018). Depending on the scenario, responders can contain the oil by using floating booms, collect it mechanically using skimmers or chemically by releasing polymers (herders), burn it or enhance dispersion by spraying surfactants on the slick. Every method has advantages and drawbacks and their applicability rely on windows of opportunity. For example, the oil can emulsify and surfactants are not as efficient as when applied upon fresh oil or the oil slick is so thin (< 2mm) that ignition is unable to occur (Fingas, 2011). The presence of sea ice is an extra obstacle in oil spill recovering actions. Skimmers can quickly become clogged with pieces of ice and the oil might not reach the required flash point to be ignited, despite being present at a sufficient thickness (Wilkinson et al., 2017).

Although spill accidents are unpredictable, nowadays decision makers often count with en-

vironment information at near-real time and regional assessments that can support faster decisions. Such assessments (*e.g.* Spill Impact Mitigation Assesment (SIMA)) are strategy plans created through the synergistic effort between researchers, industry, government authorities and society to determine which recovery method will minimize impacts of spills on shared values, such as ecosystem, local business and cultural heritage.

In the marginal ice zone, the sea surface is covered by a fragmented, cohesive sheet of ice built by floes. Spilled oil can be trapped between the floes and its drift depends on the sea ice concentration (*C*. As a rule-of-thumb dated from the 1970s and further supported by theoretical arguments (Venkatesh et al., 1990) and field experiments (Sørstrøm et al., 2010), the spilled oil tends to drift as in open waters when C is low, $C < 30\%$. For higher sea ice concentrations ($C \geq 80\%$), oil is tightly trapped between the ice floes and its drift is mainly controlled by the sea ice velocity. The transition between these two extremes is still not well established in the community and different approaches have been proposed. (French-McCay et al., 2018), for example, considered that oil travels with the ice field even in this intermediate interval whereas (Nordam et al., 2019) and (Arneborg et al., 2017), both described in 2.1.3, present a linear and probabilistic approach, respectively.

Currently, both private (*e.g.* SINTEF) and public institutes (*e.g.* the Swedish Meteorological and Hydrological Institute (SMHI)) have developed and implemented sophisticated oil-in-ice models. SINTEF, for example, developed and maintains the trajectory, fate and response Oil Spill Contingency And Response (OSCAR) (Reed et al., 1999). Nordam et al. (2019) used OSCAR to simulate the oil slick trajectory from an oil-in-ice field experiment promoted in the marginal ice zone (reported sea ice concentration between 70%–90%) of the Barents Sea in 2009 (Sørstrøm et al., 2010). The authors report good agreement between modeled and observed trajectories and they highlight the importance of considering sea ice rheology in the ice models instead of a simple sea ice free drift approach.

The Spill Impact Model Application (SIMAP)/OIL and Spill Impact MAPping (OILMAP) software, developed and maintained by the RPS ASA Group, was also used to simulate field trials in the marginal ice zone of the Barents Sea (Reed and Aamo, 1994) with sea ice concentration varying between 60% and 90%. The authors report good agreement between the observed oil slick and trajectories when the wind drift factor and turning angle were tuned depending on the intensity and direction of the winds. SIMAP was also applied to simulate hypothetical oil spills from different scenarios (well blowouts, sub-sea pipeline leak or shipping accident) in the Beaufort Sea under sea ice conditions (Gearon et al., 2014). The results indicate profound effects of the sea ice on oil behaviour, both in weathering and transport. According to the authors, oil spread less when placed in sea ice relatively to open water and weathering process are slowed. The authors also highlighted possible difficulties in clean up operations

due to the sea ice presence.

Forcing virtual particles with different ice-ocean models, French-McCay et al. (2018) used SIMAP to validate oil spill trajectories with the observations from Barents Sea field experiment and drifters from the International Arctic Buoy Program (IABP) drifters. The authors highlight better agreement between simulated and observed tracks when Elasto-Brittle rheology is used instead of the Elastic–Viscous–Plastic rheology. Moreover, they underline the necessity of using ice-ocean forcing with time steps smaller than daily and without time-averaging the input fields. Using a similar oil-in-ice model, but different ice-ocean forcing, Beegle-Krause et al. (2017) also reproduced the trajectory of IABP buoys and the field experiment and their findings converge to the ones presented by French-McCay et al. (2018).

Apart from the private companies as the ones mentioned above, public institutes are also working on the development and operationalization of oil spill models in the presence of sea ice. Together with the Danish Maritime Safety Administration (DAMSA), SMHI maintains the Seatrack Web, an internet based software used to simulate oil spills and to support response measures in the Baltic Sea and part of the North Sea (Ambjorn, 2008; Kostianoy et al., 2008). Atmospheric forcing in Seatrack Web is incorporated from the HIgh Resolution Limited Area Model (HIRLAM) and currents are obtained from the HIgh Resolution Operational Model for the Baltic (HIROMB). Arneborg et al. (2017) used Seatrack Web to reproduce the oil spill in the Baltic Sea in 2006 caused by the sinking of the Dominican-registered cargo ship Runner 4.

1.0.2 Motivation

Oil has undoubtedly been an intrinsic character of our society over the last 100 years. According to BP's world energy 2019 report (British Petroleum, 2019), oil represents about 34% of the world total primary energy consumption and it is foreseen that it will continue to be the major source of energy in the near future (Canada's Oil & Natural Gas Producers, 2018). Estimations indicate that the oil and gas industry represented approximately 3.8% of the global economy in 2019. Only in the U.S., the oil and gas industry employed 895,629 professionals in this same year (Furnans et al., 2020).

The history of Norway in oil exploitation started 51 years ago with the Ekofisk oil field discovery and since then massive revenues supported the wealthy development of the country. In 2017, oil and gas sales were responsible for approximately 40% of the Norwegian exports, accounted for about 14% of Norway's gross domestic product and directly employed approximately 86,000 people (Vatne, 2018). Furthermore, the Norwegian Petroleum Directorate (NPD) estimates that about half of the total petroleum resources in Norwegian waters

are still left to be discovered and more than 60% of that is located in the Barents Sea. The latter, specifically its northern part, was the main responsible for the 40% growth relative to the previous estimation of undiscovered resources made in 2015 by the NPD, totaling 4000 million standard cubic metres of oil equivalent (scm oe) (Directorate), 2018).

Since 2015 geophysical surveys and shallow drilling have been conducted as part of the NPD's strategic plan on mapping the North - Northeast Barents Sea for resources availability, including regions just next to Svalbard. Although neither commercial fields are currently in operation nor were included in the Awards in Predefined Areas, such exploration activities can still be seen as signal of the future plans for the region.

Simultaneously to this increase in resource interests, the ongoing reductions in sea ice extension (Serreze et al., 2007) and thickness (Wadhams and Davis, 2000) have also allowed the intensification of shipping activities in the Arctic region. The Northern Sea Route (NSR), for example, a shipping lane officially defined between Novaya Zemlya and the Bering Strait, transported 31.5 million tons of goods in 2019, 56.7% more than in 2018. A total of €143 billions of private investments is required to achieve the Kremlin's ultimate goal of 80 million tons of goods transported in the NSR by 2024 and 90 million tons by 2030.

As these activities increase further north, so does the probability of oil spills. Studies have shown that key Arctic species, such as the Polar cod (*Boreogadus saida*), can be highly impacted by oil during their embryonic and early stage development even in small concentrations, suffering from physical deformations to feeding incapacity (Nahrgang et al., 2016; Bender et al., 2021). Moreover, there are indications that the *Exxon Valdez* oil spill in 1989 might have a role in the fishery collapse in Prince William Sound, Alaska (Incardona et al., 2015).

According to the National Research Council, it is estimated that 343,200,000 gallons of oil are released every year into the sea (Transportation Research Board and National Research Council, 2003). Only in the U.S. and Canada, about 1 and 15 oil spills of more than 1000 gallons each occur in navigable waters per day, respectively (Fingas, 2012). These numbers and major spill accidents, like the *Deepwater Horizon*, naturally guide us to believe that the main inputs of oil into the sea comes from extraction or during transportation. It is estimated however that almost half of this annual input comes actually from natural seeps, regions where crude oil is released through cracks in the seafloor into the water column (Transportation Research Board and National Research Council, 2003; Fingas, 2012). It must be highlighted that the oil leaking continuously and slowly from natural seeps is an intrinsic feature present in these areas and the environment is already adapted to such a condition.

Due to these societal and environmental concerns, international cooperation initiatives have been established to improve the knowledge, models performance and response capabili-

ties. The OIL SPILL project (Enhancing oil spill response capability in the Baltic Sea Region, 2019), composed by research institutes from Finland, Latvia, Denmark, Estonia, Lithuania and other countries, aims to organize oil spill combating in coastal areas in the Baltic Sea region by training volunteers and identifying cross-border legal requirements. The Center for Spills and Environmental Hazards from the University of New Hampshire has also been promoting workshops to experts under the Arctic Spill Modeling flag to discuss the current capability, flaws and possible improvements in oil spill modeling and detection under sea ice conditions. Further information can be found at https://crrc.unh.edu/workshop/AMSM_virtual_2020.

Reliable oil-in-ice drift models, such as the ones used by French-McCay et al. (2018); Nordam et al. (2019); Arneborg et al. (2017), have been developed and extensively used over the years by the community. Nonetheless, these are usually paid softwares, and when free of charge, the source code is not open for modifications made by the user. In addition, no studies conducted so far compared the response of two distinct oil-in-ice drift approaches under a same set of simulation experiments. This work intends to fill in these two gaps by having as main objective the implementation, evaluation and comparison of two different oil-in-ice drift models in OpenDrift (Dagestad et al., 2018), an open-source Lagrangian particle tracking framework. The model formulations are the ones proposed by Nordam et al. (2019) and Arneborg et al. (2017) and they are described in Subsection 2.1.3.

The document is structured as follows: Chapter 2 presents the OpenDrift framework and the two oil-in-ice drift models implemented in it, the dataset obtained in the field experiment in the Barents Sea and the IABP data, the atmospheric and ocean-ice models used to force the virtual particles and the statistics used to evaluate the simulations. I present in Chapter 3 the results obtained and discuss them in Chapter 4. Finally, Chapter 5 synthesizes the study and presents suggestions for further studies.

Chapter 2

Methods and Data

In this chapter the Lagrangian particle tracking framework used in the research as well as the two oil-in-ice models implemented are described. Moreover, the atmospheric, ocean and ice inputs used to force the virtual particles and the datasets used to validate the simulated trajectories are presented. Finally, the statistical methods applied to evaluate the trajectories against the observed drifter tracks are described.

2.1 Methods

2.1.1 Lagrangian Particle Tracking

A fluid body as being composed of an infinite amount of particles. Each particle presents position, temperature and salinity and other properties (*e.g.* tracer concentration). In Fluid Dynamics, fluid motion can be described in two different, but corresponding ways: Lagrangian and Eulerian. In the Lagrangian description, fluid particles are followed throughout the flow field and the properties of interest are recorded or computed on each consecutive time step. In practical words, meteorological balloons and ocean buoys are examples of Lagrangian devices in the sense that they flow with the fluid motion which they were deployed in. Since the particles are tracked in the Lagrangian description, its position $\mathbf{X}$ varies in time and at a given time t it can be described by the position vector $\mathbf{X} = \mathbf{X}(t)$. As this particle moves, it traces a curve in space known as *trajectory* (van Sebille et al., 2018). The trajectory, and hence the position of the particle on the subsequent time steps, are linked to the initial position of this tracked body. In other words, if such a particle had a different position at the first time step t_0, different trajectories would be obtained. Having this said, at a later time, the position vector is given by $\mathbf{X} = \mathbf{X}(\mathbf{X}(t = t_0),\ t)$ or $\mathbf{X} = \mathbf{X}(\mathbf{a},\ t)$, where $\mathbf{a} = \mathbf{X}(t = t_0)$. In the Lagrangian description, the position vector $\mathbf{X}$ is the dependent variable and the initial position $\mathbf{a}$ and time

t are the independent variables.

The Lagrangian velocity is thus simply given by:

$$\mathbf{V}_L = \frac{d\mathbf{X}(\mathbf{a}, t)}{dt}\Big|_{\mathbf{a}} \tag{2.1}$$

On the other hand, the Eulerian description focuses on fixed points within a domain and involves four independent variables: the three spatial coordinates represented by the vector $\mathbf{x}$ and time t. Contrasting the Lagrangian devices, Eulerian equipment stay fixed in a point, such as a meteorological station or an ocean mooring, and their sensors measure the fluid properties flowing through them. The instantaneous velocity ($\mathbf{V}_E$) passing through this control volume and sampled by the device is given by

$$\mathbf{V}_E(\mathbf{x}, t)\Big|_{\mathbf{x}} \tag{2.2}$$

Putting in words, the measured variable in the Eulerian framework is independent in space (measured at the same point), but time dependent (the device measures continuously).

Since we are describing the same fluid, an observed property (F) must have the same value in both frameworks when a particle, described by Lagrangian kinematics, crosses an Eulerian point in a given position (x, y) and time t.

$$\underbrace{F[\mathbf{X}(\mathbf{a}, t)]}_{\text{Lagrangian}} = \underbrace{F(\mathbf{x}, t)}_{\text{Eulerian}} \tag{2.3}$$

Applying the total time derivative on Eq. 2.3, one obtain:

$$\frac{d}{dt}F[\mathbf{X}(\mathbf{a}, t)] = \frac{\partial F}{\partial t} + \frac{\partial F}{\partial X_1}\frac{dX_1}{dt} + \frac{\partial F}{\partial X_2}\frac{dX_2}{dt} + \frac{\partial F}{\partial X_3}\frac{dX_3}{dt} \tag{2.4}$$

since $\frac{dX_i}{dt}$ are the components v_i of the fluid particle, we can rewrite Eq. 2.4 as:

$$\frac{d}{dt}F[\mathbf{X}(\mathbf{a}, t)] = \frac{\partial F}{\partial t} + \frac{\partial F}{\partial X_1}v_1 + \frac{\partial F}{\partial X_2}v_2 + \frac{\partial F}{\partial X_3}v_3 = \frac{\partial F}{\partial t} + (\nabla F)\cdot\mathbf{v} \tag{2.5}$$

Hence:

$$\frac{d}{dt}F(\mathbf{x}, t) = \frac{\partial F}{\partial t} + \frac{\partial F}{\partial X_1}v_1 + \frac{\partial F}{\partial X_2}v_2 + \frac{\partial F}{\partial X_3}v_3 = \frac{\partial F}{\partial t} + (\nabla F)\cdot\mathbf{v} = \frac{D}{Dt}F(\mathbf{x}, t) \tag{2.6}$$

In Lagrangian particle tracking, labeled virtual drifters are released in an Eulerian numerical

grid (*e.g.* ocean model) and their position are tracked over the simulation. Moreover, properties (density, diameter, viscosity *etc*) can also be provided to the virtual particles and these are equally tracked. As we saw before, when $\mathbf{X}(t) = \mathbf{x}$, Lagrangian and Eulerian velocities are the same and since the seeded virtual elements are within an Eulerian domain, we can use the latter velocities to update particle positions from t to $t + \Delta t$ (van Sebille et al., 2018).

When using an ocean or atmospheric model, the Lagrangian integration can be done in two different ways: *online* and *offline*. The first occurs when trajectories are computed at each time step that the Eulerian model is updated. In the *offline* approach, on the other hand, the Lagrangian particles are forced by stored fields obtained previously. One of the advantages in the latter approach is that one can use different models to perform the same simulation scenarios. Regardless the choice, the following equation is used to update the particle positions:

$$\underbrace{\mathbf{X}(t+\Delta t)}_{\text{Next position}} = \underbrace{\mathbf{X}(t)}_{\text{Current position}} + \underbrace{\int_t^{t+\Delta t} \mathbf{v}(\mathbf{x}(\tau),\tau)\,d\tau}_{\text{Eulerian velocity}} \tag{2.7}$$

where τ is time in the Eulerian domain (van Sebille et al., 2018). Solving Eq. 2.7 might look straightforward, but one must remember that integration must happen in time and the forcing variables in the Eulerian grid must be interpolated to the particle positions, and both procedures are inherently imperfect thus adding errors in the simulation. A thorough review of the topic can be found in van Sebille et al. (2018) and the Lagrangian mathematical formalism in Bennett (2006).

The offline Lagrangian particle tracking approach has been widely used to simulate the trajectory of floating objects in ocean, such as marine floating litter (Pereiro et al., 2018), oil spills (Androulidakis et al., 2020), sea ice (Rampal et al., 2016), egg and larvae drift (Romagnoni et al., 2020), transport of sediment (Devis-Morales et al., 2021) and others.

2.1.2 The Offline Lagrangian Framework - OpenDrift

For this work, I was used the open-source Lagrangian particle tracking framework developed at the Norwegian Meteorological Institute, OpenDrift (Dagestad et al., 2018). Coded in Python and made available on https://opendrift.github.io/install.html, OpenDrift contains different modules, including an oil spill drift and fate model, the OpenOil (Röhrs et al., 2018). Composed by sub-modules that describe the different transport and the weathering processes that take place after an oil spill has occurred, OpenOil uses tabulated oil information provided by the Norwegian Clean Seas Association for Operating Compa-

nies (NOFO) and is also linked to the oil library used by PyGNOME (https://github.com/NOAA-ORR-ERD/PyGnome), the National Atmospheric and Ocean Administration (NOAA) oil model. Moreover, OpenDrift is CF-compliant, *i.e.*, it is compatible to the Network Common Data Form (NetCDF) in both input and outputs.

The horizontal transport of oil in OpenOil is essentially described by Eq. 1.1. The first term on the right-hand side ($\mathbf{v}_{water}$), mentioned before simply as ocean currents, can in fact be decomposed into sub-terms such as geostrophic currents, Ekman currents, Stokes drift, tidal currents and a stochastic term accounting for the unresolved subgrid-scale processes.

$$\mathbf{v}_{water} = \mathbf{v}_{geostrophic} + \mathbf{v}_{Ekman} + \mathbf{v}_{Stokes} + \mathbf{v}_{tides} + R(2K_h r^{-1} dt^{-1})^{\frac{1}{2}} \tag{2.8}$$

Where R is a random number with mean 0 and standard deviation $r = 1$, K_h is the turbulent horizontal diffusivity coefficient ($m^2\ s^{-1}$) and dt is the simulation time-step (s) (van Sebille et al., 2018; Pereiro et al., 2018). Generally saying, Stokes drift is indeed essential for oil spill modeling in ice free regions (Jones et al., 2016), but its role diminishes as the sea ice concentration increases Tuomi et al. (2018). Given the scope of this work, the Stokes drift is not considered in the simulations.

The second term in Eq. 1.1, presented as (f× $\mathbf{v}_{wind}$), is often denoted as *windage*. The windage factor (f_w) is an additional wind drag force added to the already considered ocean currents advection as a compensation to the inability of ocean models to represent motions in the very upper centimeters of the ocean (Röhrs et al., 2018; French-McCay et al., 2018; Tamtare et al., 2021). The value of f_w is considered to be somewhere between 0% and 6% (Nordam et al., 2019), with 2% and 3% as the factors most commonly used (Simecek-Beatty, 2011; Jones et al., 2016). For the simulations performed in this work, a windage factor of 3% was used, the same as found by (Faksness et al., 2010) in the field experiment conducted in the Barents Sea in 2009.

Oil droplets can be entrained into the water column due to wave breaking. Within the ocean, the droplets are subject to buoyancy and turbulent vertical mixing. The former, which is controlled by the droplet size distribution and by the difference of density between the oil and the water, can be described as a terminal vertical rise velocity as a function of the Reynolds number (Tkalich and Chan, 2002). The latter is described as a random walk scheme proposed by Visser (1997) with vertical turbulent diffusivity imported from ocean models or parameterized from the windspeed.

OpenOil was successfully used in the Gulf of Mexico to simulate the Deep Horizon Oil Spill (Hole et al., 2019), to investigate the effects of ocean dynamics on hydrocarbon transport in the Straits of Florida (Androulidakis et al., 2020) and to evaluate the potential of oil spills

around Cuba (Hole et al., 2021). A thorough description of OpenOil can be found in (Dagestad et al., 2018), (Röhrs et al., 2018) and (Jones et al., 2016).

2.1.3 Oil-in-ice models

In the OpenOil old versions, oil-in-ice interactions were restricted to particles deactivation when these reached a certain sea ice concentration threshold. The two oil-in-ice models implemented and used for this work were proposed by Arneborg et al. (2017) and Nordam et al. (2019) and are described below.

As mentioned in the previous chapter, the horizontal surface drift of oil in sea ice covered areas might be described by the "30/80" approach. Based on this rule-of-thumb, Nordam et al. (2019) proposed that the oil velocity ($\mathbf{v}_{oil}$) is composed by a combination between ice velocity ($\mathbf{v}_{ice}$), ocean currents ($\mathbf{v}_{water}$) and a wind factor ($\mathbf{f}_w\,\mathbf{v}_{wind}$), weighted by a dependent sea ice concentration coefficient (κ_{ice}), as follows:

$$\mathbf{v}_{oil} = \kappa_{ice}\mathbf{v}_{ice} + (1-\kappa_{ice})(\mathbf{v}_{water} + f_w\mathbf{v}_{wind}) \tag{2.9}$$

where

$$\kappa_{ice}\begin{cases} 0, & if\, C < 30\% \\ \frac{C-30\%}{80\%-30\%}, & if\ 30\% \le C < 80\% \\ 1, & if\, C \ge 80\% \end{cases}$$

I highlight in advance that no explicit solution is provided by Nordam et al. (2019) for the case when oil is located under the ice layer. Nonetheless, this gap is somehow filled by the model proposed by Arneborg et al. (2017) and described below. Heavily based on laboratory experiments (e.g., Cox and Schultz, 1981), oil particles under ice ($\mathbf{v}_{oil,ui}$) drift with the interior ocean currents as long as the difference between ice and water velocities exceeds a certain threshold ($\mathbf{v}_{thres}$):

$$\mathbf{v}_{oil,ui}\begin{cases} \mathbf{v}_{ice}, & if\ |\mathbf{v}_{water} - \mathbf{v}_{ice}| < \mathbf{v}_{thres} \\ \mathbf{v}_{water}, & if\ |\mathbf{v}_{water} - \mathbf{v}_{ice}| \ge \mathbf{v}_{thres} \end{cases}$$

Cox and Schultz (1981) point out that, in general terms, the oil under the ice remains attached to it until the current velocity relative to the ice reaches the range of 0.15 m s^{-1} to 0.25 m s^{-1}. Following Arneborg et al. (2017), I will use 0.2 m s^{-1} as the velocity threshold ($\mathbf{v}_{thres}$). Despite its simplicity, this expression is a clear limitation in the model formulation since sea

ice bottom roughness information is usually not provided by ocean-ice coupled models.

In addition, Arneborg et al. (2017) also takes into account the vertical migration (resurfacing) and horizontal displacement of particles within the water column, from a position below the ice to an ice-free region, for instance. Oil situated under the ice (either in contact with the ice or free in the water) may drift to an ice-free region if the horizontal oil velocity ($\mathbf{v}_{oil}$) is different from the ice drift ($\mathbf{v}_{ice}$). The probability (**P**) that it will happen depends on the distance (Δs = ($|\mathbf{v}_{oil}$ - $\mathbf{v}_{ice}|$)$\times\Delta$ t) traveled by the particle during a given time-step Δt and on the ice floe length scale ($\mathscr{L}_{floe}$). The probability that a particle will remain under the ice is given by:

$$\mathbf{P}(below\ ice \longrightarrow below\ ice) = \exp\left(-\frac{\Delta s}{\mathscr{L}_{floe}}\right) \tag{2.10}$$

The probability of a particle migrating to an ice-free region is hence given by:

$$\mathbf{P}(below\ ice \longrightarrow not\ below\ ice) = 1 - \exp\left(-\frac{\Delta s}{\mathscr{L}_{floe}}\right) \tag{2.11}$$

Conversely, the probability of a particle migrating from an ice-free position within the water column to below the sea ice is given by:

$$\mathbf{P}(not\ below\ ice \longrightarrow below\ ice) \begin{cases} 1 - \exp\left(-\frac{C\Delta s}{(1-C)\mathscr{L}_{floe}}\right), & z_p < -h_{ice} \\ 0, & z_p \geq -h_{ice} \end{cases}$$

where z_p is the particle depth and h_{ice} is the ice draft.

Another difference between the two models relates to the drift of oil particles at the ocean surface in the presence of sea ice. Although also relying on the "30/80" rule-of-thumb, Arneborg et al. (2017) proposes a more probabilistic approach in the interval 30% ≤ C < 80%. The probability of a particle changing its state from *free* $\longrightarrow$ *attached* (to the sea ice), or *attached* $\longrightarrow$ *free*, is based on the particles state (free) and on the change of sea ice concentration values from the previous (C_1) to the current (C_2) time step.

As an example, if the sea ice concentration increases from C_1 to C_2, the probability that a particle that moves freely becomes attached to the sea ice is given by:

$$\mathbf{P}(free \longrightarrow attached) \begin{cases} \frac{f(C_1)-f(C_2)}{f(C_1)}, & C_2 > C_1 \\ 0, & C_2 < C_1 \end{cases}$$

where *f(C)* is the fraction of particles in free drift at a given sea ice concentration *C*. Con-

versely, if $C_1 > C_2$, none of particles will get attached to the sea ice, but the ones that are already attached might start moving freely and this probability is given by:

$$\mathbf{P}(attached \longrightarrow free) \begin{cases} 0, & C_2 > C_1 \\ \frac{f(C_2)-f(C_1)}{1-f(C_1)}, & C_2 < C_1 \end{cases}$$

Similarly to Nordam et al. (2019), Arneborg et al. (2017) also considers that particles will move as almost without sea ice and mostly attached to it for $C < 30\%$ and $\geq 80\%$ respectively.

2.2 Data

2.2.1 Field Experiment

A large field-experiment (FEX09) took place in the Barents Sea marginal ice zone in May 2009 as part of the Oil-in-ice Joint Industry Program (JIP) (Sørstrøm et al., 2010). 7000 liters of fresh Troll B crude oil were released uncontained in 70-80% ice coverage on the 15th of May and were monitored for the next 6 days. Meteorological, ocean and ice floe tracking data obtained during the field experiment were kindly provided by SINTEF and are presented in Table 2.1.

Table 2.1: Meteorological and ocean variables obtained during the FEX09 and provided by SINTEF. After Faksness et al. (2010)

Parameter	Source
Air temperature [°C]	*R.V. Lance*
Wind direction [°]	*R.V. Lance*
Wind speed [m s^{-1}]	*R.V. Lance*
Water temperature [°C]	Seaguard RCM / RDCP600
Salinity	Seaguard RCM / RDCP600
Current speed [m s^{-1}]	Seaguard RCM / RDCP600
Current direction [°]	Seaguard RCM / RDCP600

Two different GPS systems were initially considered to track ice floe drifts around the oil spill. The Garmin Astro 220 presented better reliability and was taken as the primary system while the Trackstick Pro was taken as a backup. A full description of the equipment can be found in Faksness et al. (2010). The data from the 10 GPS trackers deployed in the field experiment were combined into one "mean" trajectory and linear interpolation was used in periods with no data. The final dataset spans from the 14th of May 2009 to 20th of May 2009, with 10 minutes time step (Figure 2.1).

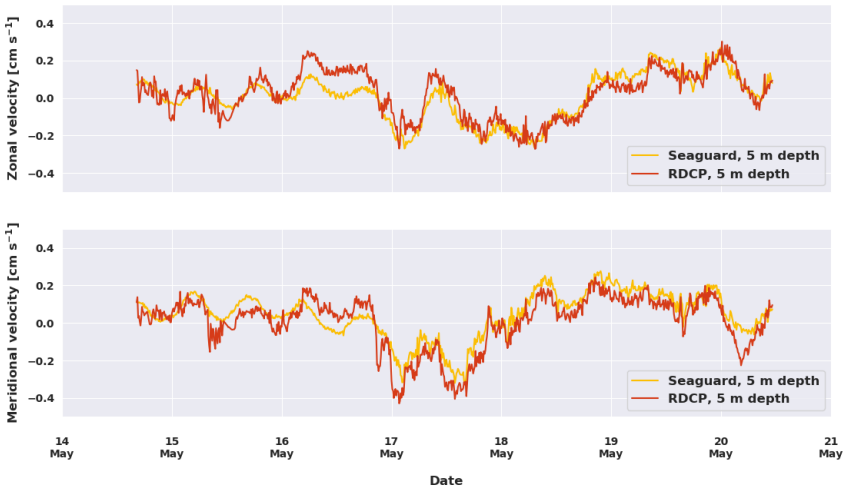

Figure 2.1: Zonal component (top panel) and meridional component (bottom panel) of current velocities [cm s^{-1}] measured at 5 m depth by a Seaguard (yellow line) and RDCP (red line) during the FEX09 experiment (Sørstrøm et al., 2010). The data was cordially provided by Dr. Tor Nordam and SINTEF Ocean.

It must be highlighted though that despite the oil slick surface area was estimated by aerial surveillance and field observations together with the GPS track data, we did not have access to it. Thus, a quantitative comparison between surface slick area provided by the oil-in-ice models and the observed one might be somehow impractical. Nonetheless, the researchers pointed out that the oil drifted with the sea ice and it remained contained between the floes throughout the whole experiment. In other words, because of this observation, we are able to use sea ice velocities derived from the GPS drifters and from ice models to simulate the oil trajectory.

2.2.2 IABP Data

According to International Tanker Owners Pollution Federation, the number of medium (7-700 tonnes) and large (> 700 tones) spill accidents involving tanker ships has been decreasing since the series started in 1970 (The International Tanker Owners Pollution Federation, 2020). Controlled field experiments and oil spill accidents provide essential data to researchers investigate models accuracy, uncertainties, parameters tuning and new algorithms development.

Nonetheless, as highlighted by Wilkinson et al. (2017), ice covered regions present lower data availability than open water seas and this gap of *in-situ* observations is also expressed as a lack of consolidated knowledge of how oil behaves in the presence of sea ice. In order to overcome this obstacle, we decided to validate the simulated spill trajectories against the observed drift of buoys from the International Arctic Buoy Program (IABP). This approach

was also applied in the field experiment that took place in the Barents Sea in 2009 (Sørstrøm et al., 2010) and Nordam et al. (2019) showed that the oil drift can be simulated by reproducing buoy trajectories with modeled ice velocities. French-McCay et al. (2018) also used IABP buoys to evaluate an oil-in-ice drift model forced by different coupled ocean-ice models.

In this sense, 1981 drifters were downloaded on the IABP server (https://iabp.apl.uw.edu/WebData/) and from these, 140 started recording during the period of interest, November - April (2018/2019, 2019/2020). These files are described by IABP as *Level 1* data, meaning that quality control and data processing measures must be applied. In this sense, the following procedures were considered:

Impossible date test: IABP day of the year (DOY) is defined within 1.0 and 365.999. Data off this range are removed.

Impossible location test: Data points outside the ranges -180 ≤ LON ≤ 180 or -90 ≤ LAT ≤ 90 are removed.

Check duplicated dates: Duplicated dates are removed from the time series.

Identify and remove spikes: Spikes were identified following the ARGO quality control test (Wong et al., 2020) defined as:

$$Test = \left| V2 - \frac{V3 + V1}{2} \right| - \left| \frac{V3 - V1}{2} \right| \tag{2.12}$$

Where *V2* is the measurement under evaluation and *V1* and *V3* are the measurements one time-step before and after, respectively. Originally, this procedure is applied on temperature (*T*) and salinity (*S*) profiles and a point *V2* is considered as a spike when:

T > 6°C for pressures less than 500 dbar or T > 2°C for pressures greater or equal to 500 dbar;

S > 0.9 PSU for pressures less than 500 dbar or S > 0.3 PSU for pressures greater or equal to 500 dbar.

In this work, a points is flagged as spikes when their magnitude is ≥ $\mu + 4\sigma$, where μ is the average of all *V2* values and σ is the standard deviation. The method was able to detect large and small peaks, but false positive and false negative points were also obtained.

Visual inspection: Considering the item before and as recommended by Thomson and Emery (2014), the time series were also visually inspected in a 'click-and-pick' interactive window. By doing this, I was able to unflag false positive points, flag the false negative ones and identify highly compromised time series.

Filtering and resampling: After properly flagging spikes and other erroneous data, the latitude and longitude time series were filtered using a median filter with a window length of 5 points and the flagged values were substituted by the filtered ones. Finally, time series sampling periods were standardized in 1 hour.

From the 140 drifters, 52 tracks were disregarded after the quality control and data processing steps. The remaining 88 trajectories were evaluated against sea ice concentration observations in order to ensure that their displacement occurred in sea ice conditions. For this, I used the sea ice concentration product of the European Organisation for the Exploitation of Meteorological Satellites (EUMETSAT) Ocean and Sea Ice Satellite Application Facility (OSI-SAF). Under the responsibility of the Norwegian Meteorological Institute (MET) and the Danish Meteorological Institute (DMI), brightness temperature data are obtained by an Advanced Microwave Scanning Radiometer 2 instrument (AMSR-2), with subsequent atmospheric corrections and application of algorithms on the corrected data to retrieve sea ice concentration. This OSI-SAF daily product has a horizontal resolution of 10 km and it was spatially interpolated in the observed trajectories on the first 15 days of drift.

It is presented in Figure 2.2 the drifter trajectories before (*a*, 140 beacons) and after (*b*, 88 beacons) the quality control and data processing procedures, with their initial position represented by red dots: red trajectories represent the ones which their first 15 days of drift happened in open waters (33), neglected in this work, and black trajectories are those which sea ice was present, hence considered hereinafter (55).

2.2.3 Wave Sensors Deployed in the Marginal Ice Zone

Between 12 and 14 September 2018 occurred the fourth Nansen Legacy (AeN) research cruise. Conducted on the north of Spitsbergen, 4 wave sensors were deployed on ice floes and monitored until their shutdown. It is presented in Figure 2.3 the observed trajectories of the four sensors (14432, 14435, 14437 and 14438) superimposed over the time averaged sea ice concentration map obtained from RIOPS and TOPAZ4-H models for the study period (19.09.2018 - 01.10.2018).

These were deployed in the context of the Nansen Legacy Project, during the September 2018 cruise, from the research vessel *R.V. Kronprins Haakon*. The deployment took place in the MIZ of the Barents sea on September 19th 2018, around 250km North of Svalbard. During deployment, the icebreaker was steaming perpendicular to the estimated ice edge, towards regions of higher ice concentration. As a consequence, the first instrument was deployed on a solitary ice floe in the outer MIZ, while the second was set in dense drift ice, the third at the beginning of closed drift ice, and the fourth further inside the pack ice.

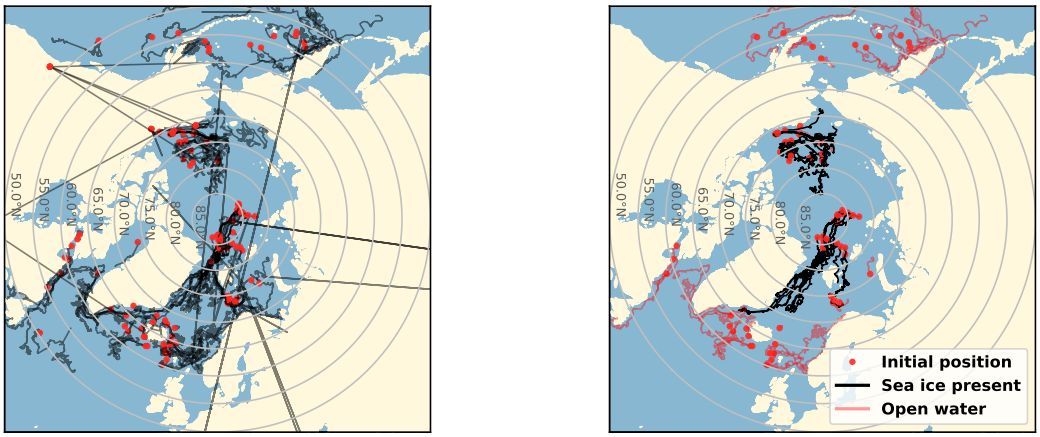

(a) (b)

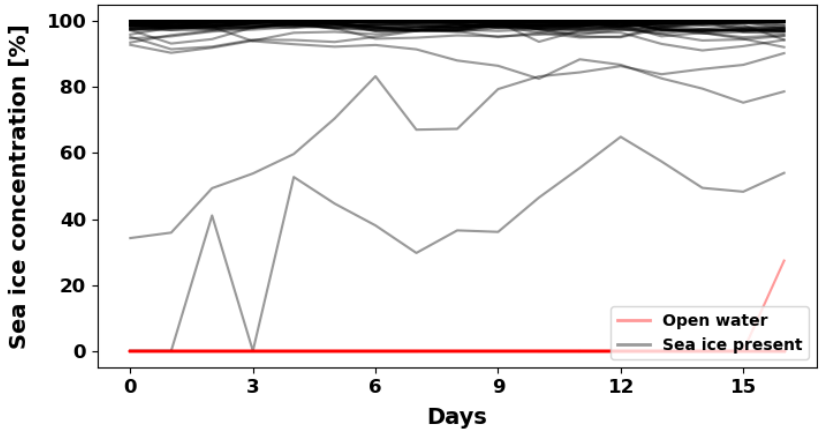

(c)

Figure 2.2: IABP drifters before (a, 140 trajectories) and after (b, 88 trajectories) data processing and quality control. Red dots represent their deployment position. Panel (c) shows sea ice concentration values from OSI-SAF interpolated to drifters in (b) over their first 16 days. The colors of trajectories in (b) represent the presence (black) or absence (red) of sea ice, as shown by the same colors in (c).

Each instrument features a high accuracy Inertial Motion Unit (IMU), in the present case the VN100 from Vectornav (Corporation, 2019), which has been used in a number of previous works (Rabault et al., 2017; Marchenko et al., 2017; **?**; Sutherland and Rabault, 2016). While the design of the instruments is focused towards measurements of waves in ice, each of them also includes a GPS that provides accurate localization. Finally, an Iridium modem is used to remotely transmit the data. In the following, the tracking feature of the instruments will be exploited. As the instruments were deployed on ice floes, they effectively allow to monitor the Lagrangian ice drift. Transmission of data happens with a period of around 5 hours. Therefore, highly resolved drift trajectories are available, as visible for example in Figure 2.3. As the instruments are equipped with large batteries and solar panels, trajectories should in theory be available for long periods of time. However, in practice, a large storm incoming

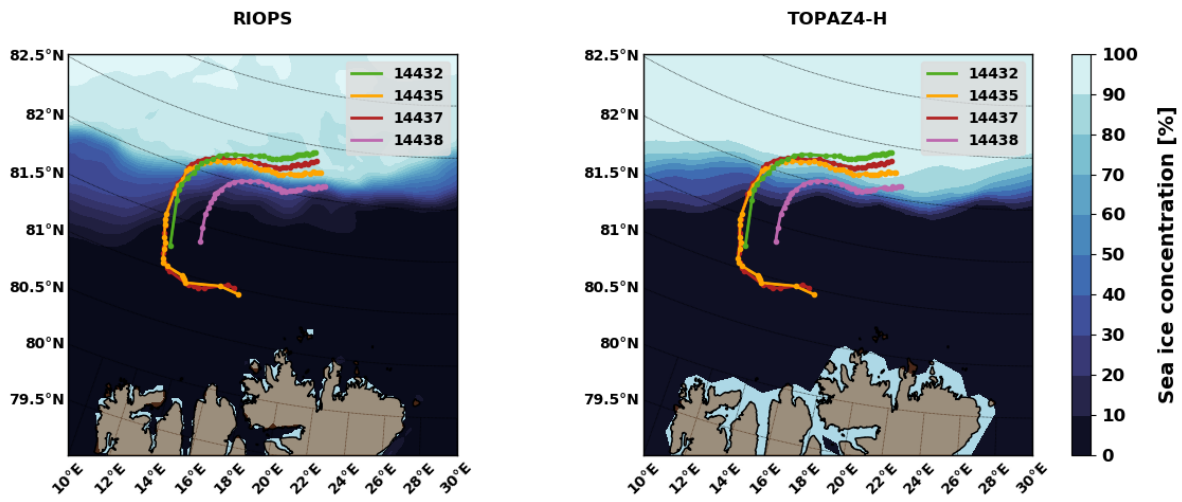

(a) (b)

Figure 2.3: Nansen Legacy (AeN) drifters deployed in the Barents Sea marginal ice zone in 2018 (coloured lines) superimposed to the mean sea ice concentration fields obtained from RIOPS (a) and TOPAZ4-H (b).

from the Northern Atlantic ocean led to loss of contact after around 2 weeks for the instrument that survived longest. Over the corresponding period of time, the total drift length is about 340 km (Rabault et al., 2019).

2.2.4 Atmospheric and Ocean Forcing

As an offline framework, particles in OpenOil are forced by external outputs. Different set of experiments were proposed (see Subsection 2.3) and due to non-overlapping periods, distinct products are used to perform the simulations. These are described as follows.

Two different ocean-sea ice models were used for the IABP and AeN trajectory simulations, the operational version of Towards an Operational Prediction system for the North Atlantic European coastal Zones *v.* 4 (Sakov et al., 2012) (TOPAZ4) and the Canadian Regional Ice and Ocean Prediction System (RIOPS) (Dupont et al., 2015). The first is available at Copernicus Marine Environment Monitoring Service (2018) while the outputs from the latter can be downloaded at http://dd.alpha.weather.gc.ca/yopp/. Moreover, atmospheric forcing for the simulations were obtained from the Canadian Arctic Prediction System (), which outputs can also be found in the latter data server.

TOPAZ4 is a coupled ice-ocean data assimilation system for the North Atlantic and the Arctic based on Ensemble Kalman Filter (EnKF) with 100 dynamical members (Sakov et al., 2012). The EnKF is used to assimilate data from both satellite and *in situ* measurements in near real time and from reanalysis products. Its hydrodynamic model (HYCOM *v.* 2.2.18) is cou-

pled with the Los Alamos Sea Ice Model (CICE) and with an ecosystem model, the ECOSMO (Schrum et al., 2006). Covering the whole Arctic with a resolution between 12.5 and 16 km (1/8°), TOPAZ4 was developed and is maintained by the Nansen Environmental and Remote Sensing Center (NERSC) and runs operationally for the Arctic – Monitoring Forecasting Centre of the Copernicus Marine Environment Monitoring Service (CMEMS ARC-MFC) at the Norwegian Meteorological Institute (Simonsen et al., 2019). Inheriting CICE's functionalities, TOPAZ4 presents an elastic-viscous-plastic (EVP) sea ice rheology Hunke and Dukowicz (1997). Hereinafter, I will refer to this hourly product as TOPAZ4-H.

Developed and maintained by the Environment and Climate Change Canada (ECCC) as a contribution to the Year of Polar Prediction (YOPP), RIOPS provides 48 hrs ice and ocean forecasts four times a day for the region situated between the Bering Strait to 26°N in the North Atlantic Ocean. With a spatial resolution between 3 and 8 km (1/12°) and hourly averaged surface fields, RIOPS ice-ocean initial conditions are downscaled from the Global Ice and Ocean Prediction System (GIOPS Smith et al., 2016). The RIOPS ocean model engine is the Nucleus for European Modelling of the Ocean (NEMO *v.* 3.6) and the sea ice model is CICE 4.0, with the same sea ice rheology as TOPAZ4 (EVP). In fact, RIOPS is an extension of the Regional Ice Prediction System (Lemieux et al., 2016) and as such, RIOPS also counts with data assimilation of sea ice concentration from passive microwave satellites.

RIOPS is coupled with CAPS and the latter provides the atmospheric forcing to the ice-ocean model system. CAPS is downscaled from the Global Deterministic Prediction System (GDPS), also developed and maintained by ECCC, and presents a spatial grid resolution of 3 km covering the whole Arctic. TOPAZ4-H, on the other hand, is forced at the sea surface by the European Centre for Medium-Range Weather Forecasts (ECMWF) operational analysis. With a horizontal resolution of 0.1° x 0.1°, ECMWF provides atmospheric fields such as dew point temperature, sea level pressure, air temperature at 2 m height and wind speed at 10 m height to TOPAZ4.

In order to reproduce the FEX09 experiment and the hypothetical oil spill (see third experiment, Section 2.3), different inputs were used, namely the TOPAZ4 reanalysis, the Nordic Seas 4 km numerical ocean model hindcast archive (SVIM Lien et al., 2013) and the NORA3 product as atmospheric and wave forcing (Haakenstad et al., 2021). The first, referred from now on as TOPAZ4-R, extends from 1991 to 2018. With daily mean outputs, it is initialized in 1979 with the World Ocean Atlas climatology and it is forced at the ocean surface by the 5° ECMWF ReAnalysis (ERA5). TOPAZ4-R also counts with a data assimilation system and its horizontal resolution and sea ice rheology are the same as the operational version (TOPAZ4-H), *i.e.*, 12.5-16 km and EVP, respectively (Xie and Bertino, 2021). The data set is freely available at Copernicus Marine Environment Monitoring Service (2018) as well.

SVIM is 4 km horizontal resolution model hindcast that covers the period between 1960 - 2018 (Lien et al., 2013). The model domain extends from the Nordic Seas to parts of the Arctic Ocean, including the Barents Sea, Pechora Sea and the Kara Sea and provides daily outputs. The model core is based in the Regional Ocean Modeling System (ROMS), with 32 vertical sigma levels and is force at the ocean surface by the NOrwegian ReAnalysis 10km (NORA10). Oceanic initial and boundary values were derived from the Simple Ocean Data Assimilation dataset version 2.1.6 (SODA 2.1.6) whereas for sea ice they were obtained from MICOM (Miami Isopycnic Coordinate Ocean Model). The ice dynamics is also based on the EVP rheology and the tidal forcing on TPXO4.

The last product considered in this work is NORA3 (Solbrekke et al., 2021; Haakenstad et al., 2021), a new atmospheric hindcast that covers the Norwegian Sea, the North Sea, the Barents Sea and part of the Arctic Ocean. NORA3 is an ERA5 dynamically downscaled product obtained by using the 3 km horizontal resolution, nonhydrostatic numerical weather prediction model HARMONIE-AROME. The hindcast outperformed NORA10 and ERA5 in the reproduction of maximum wind speed observed in 12 out of 19 polar low centers and in the representation of near-surface winds over open ocean and coastal terrains (Haakenstad et al., 2021).

2.3 Oil Spill Simulations

I have defined 3 set of experiments to conduct the simulations. The first aims to reproduce the oil trajectory observed in the field experiment (FEX09). Virtual particles were forced with the ice-ocean outputs imported from TOPAZ4-R and SVIM. No vertical motions or weathering are considered in the simulations. Wind measurements made during FEX09 were used as forcing.

The second experiment intended to replicate the selected IABP and AeN drifter trajectories. For these simulations, atmospheric forcing was provided by CAPS and ocean-ice inputs from TOPAZ4-H and RIOPS. Similarly to the first experiment, simulations were also 2D and no weathering processes were considered. Two different procedures are used:

. Release of 1000 virtual particles at the initial position of every drifter and advect them for 15 days.

. Release of 1000 virtual particles along the drifters track, restarting the simulation every 3 days and advecting particles for also three days.

The same approach will be used for the drifters released in the Barents Sea during the Nansen

Legacy cruise. I highlight however that the observed drifters had a shorter life span (between 7 and 12 days), so the simulations will last for the drifter's corresponding time length.

The last experiment was hypothesized to simulate an oil spill accident in the Barents Sea and it intends to use the oil-in-ice drift outputs as a source of information to mitigation assessments. The chosen hypothetical oil spill site is located in the Pechora Sea, next to the Kara Gate (Figure 2.4).

The position was not however chosen randomly. Backtrack studies (e.g. Huserbråten et al., 2019) have supported evidences that Polar cod (*Boreogadus saida*) spawning areas in the Barents Sea seem to be split in at least two different regions with one of them being located in the Pechora Sea, more precisely in the vicinity of Kara Gate. The research also highlights that this spawning assemblage appears to be the most important in recruitment variability in the Barents Sea. Furthermore, Polar cod early life history is closely associated with sea ice (Laurel et al., 2019) and hence an oil spill accident between December - April could directly impact individuals during their incubation period and early development.

Although not officially part of the Northern Sea Route, the Kara Gate is one of the passages which tankers cross to access western Europe. Part of the oil is exploited in the Novoportovskoye oil field, in the Yamal Peninsula, with a distribution terminal located offshore near the Cape Kamenny in the Gulf of Ob of the Kara Sea (Bambulyak et al., 2015). Since 2016, Novy Port crude oil is offloaded all-year-round at the Arctic Gates terminal to ice-class (Arc7) shuttle tankers of about 42 thousand deadweight tonnes and transported through the Kara Gate to a transhipment terminal in the Kola Bay of the Barents Sea for further delivery to European refineries.

It is shown in Figure 2.4 the monthly mean (March, April and May) sea ice concentration distributions (30% and 80%) in the Barents and Kara Sea from 1979 to 2020 using the National Snow and Ice Data Center (NSIDC) Sea Ice Index version 3 dataset (Snow and (NSIDC), 2017). As one can observe, and also pointed out by other researches (e.g. Onarheim and Årthun, 2017), the sea ice extent has been significantly retreating over the years in the Barents Sea and on its marginal seas, even in March and April when the sea ice reaches its maximum extent. Such a decrease might promote an intensification of maritime traffic in the area, thus also possibly increasing the probability of shipping and oil spill accidents.

For this experiment, a set of stochastic runs was performed (240) by randomly initializing the simulations in different start dates between March and May (1998 - 2017) and varying coefficients (windage factor and horizontal diffusion) for every run. 100 particles were released for each of the 2D oil spill simulations and they were forced for 10 days by the SVIM and TOPAZ4-R ice-ocean fields, with wind inputs from the NORA3 hindcast. I expect to obtain with this experiment a probability map of the distribution of particles and, given the

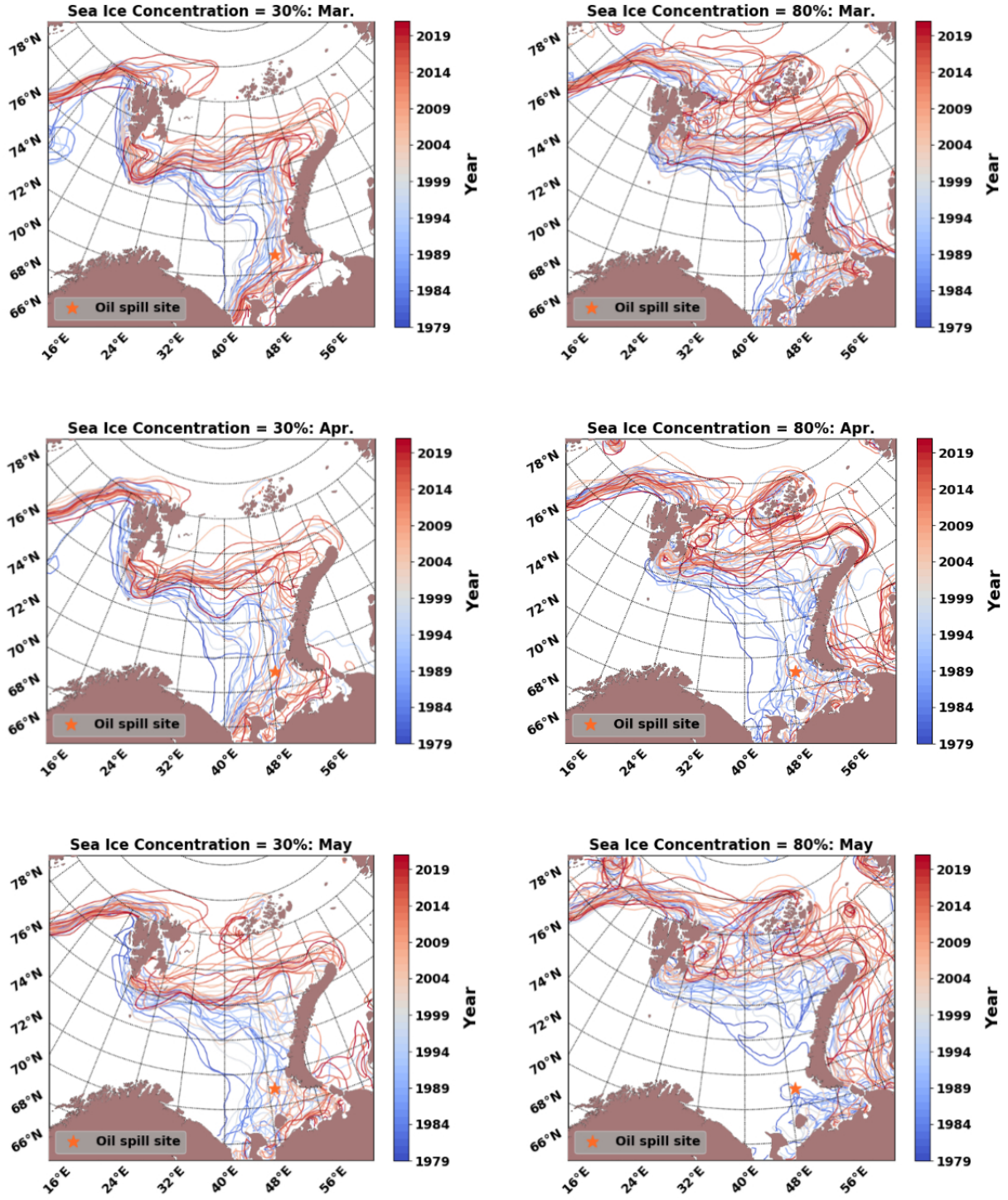

Figure 2.4: Sea ice concentration maps for 30%, and 80% using the NSIDC Sea Ice Index monthly mean data (March, April and May), Version 3, for the 1979 - 2020 period. The oil spill site is represented by the orange marker.

release position, evaluate the temporal variability of trajectories (spreadness and distance travelled).

2.4 Statistics

2.4.1 Cumulative Lagrangian Separation Distance

In order to evaluate the accuracy of the simulated trajectories in first and second experiments, the normalized cumulative Lagrangian separation was applied (Liu and Weisberg, 2011). This metric is based on the ratio between the normalized cumulative separation distance (d) and the cumulative length of the observed trajectory (dl):

$$s = \frac{\sum_{i=1}^{N} d_i}{\sum_{i=1}^{N} dl_i} \tag{2.13}$$

where d_i is the separation distance between the modeled and the observed points of the trajectories at time step i after the model initialization ($i = 0$), dl_i is the length of the observed trajectory and N is the total number of points.

The skill score is given by:

$$ss = \begin{cases} 1 - \frac{s}{n}, & \text{if } s \leq n \\ 0, & \text{if } s > n \end{cases}, \text{where } n \text{ is a tolerance threshold.} \tag{2.14}$$

The tolerance threshold $n = 3$ was considered. It means that results with cumulative separation values larger than 3 times the cumulative length of the observed trajectory are considered to be no skill. Although the choice of such threshold is arbitrary, it defines the expectations or requirements to the model (Liu et al., 2014). The perfect fit between modeled and observed trajectories occurs when the distance d_i is zero ($s = 0$) and hence $ss = 1$.

Chapter 3

Results

This section presents the results of the three experiments described before. In Subsection 3.0.1, the simulations of the field experiment that took place in the Barents Sea marginal ice zone in 2009 (FEX09) are presented. In Subsection 3.0.2 the analysis of the IABP buoys and the Nansen Legacy drifters simulations forced by RIOPS, TOPAZ4-H and CAPS is shown. Lastly, Subsection 3.0.3 contains the outputs of the hypothetical oil spill in the Pechora Sea when virtual particles were forced by SVIM, TOPAZ4-R and NORA3.

3.0.1 Oil Field Experiment in the Barents Sea MIZ - FEX09

Figure 3.1 shows trajectories when particles were forced by sea ice velocity derived from the GPS drift. The orange star represents the release position, the solid, black line is the observed trajectory and the red and green lines represent the simulations ran with the Nordam et al. (2019) and Arneborg et al. (2017) oil-in-ice drift approaches, respectively. It can be observed, as expected, that OpenOil satisfactorily reproduces the observed drift when both of the oil-in-ice approaches was used.

In Figure 3.2, particles were forced with ice velocities and ocean currents from TOPAZ4-R (left) and SVIM (right), but winds obtained *in situ*. The background map represents the mean sea ice concentration for the study period (14/05/2009 - 20/05/2009) from the two ice-ocean models and the red and yellow lines mark the position of C = 80% and 30% respectively, at the first (dashed) and last (solid) time steps. One can observe that in both cases the modeled trajectories vaguely matched the observed one, drifting southwards right after the releasing. Their total displacement is however shorter (TOPAZ4-R: -60%; SVIM: -30%) than the recorded drift (101 km). Moreover, while the drift models do present different trajectories when forced by TOPAZ4-R, they are essentially the same with SVIM.

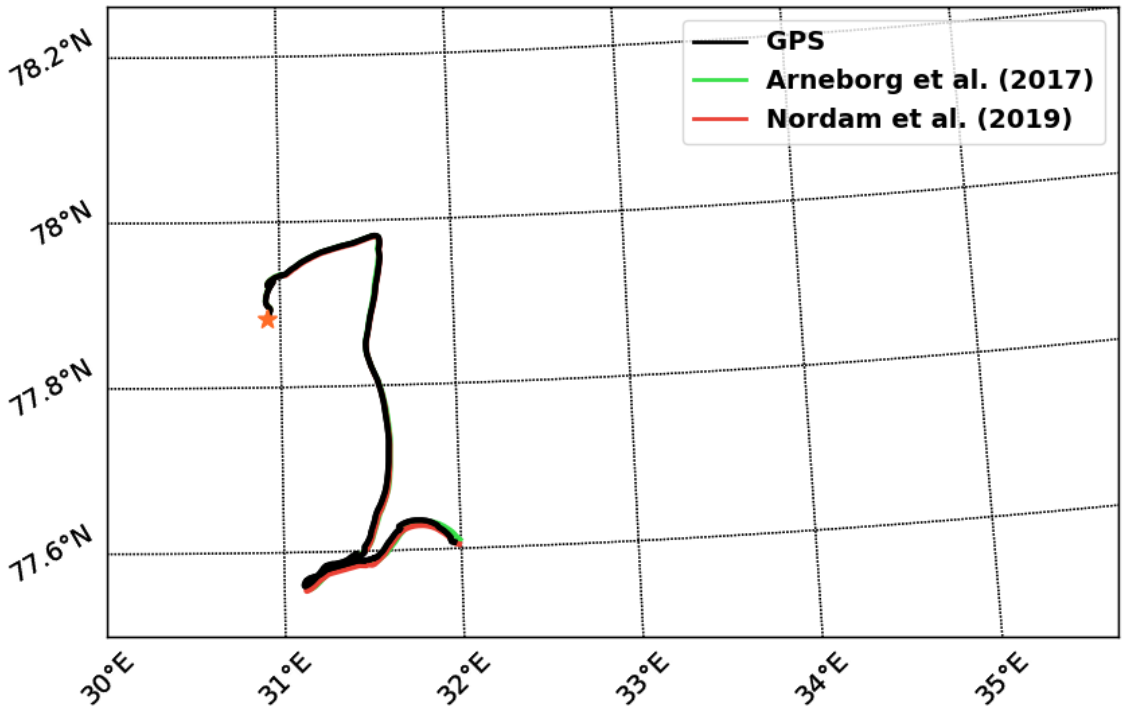

Figure 3.1: Observed GPS drift (black line) obtained during the FEX09. The red (green) line represents the modeled trajectory using the Nordam et al. (2019) (Arneborg et al. (2017)) oil-in-ice approach. Particles were forced with the sea ice velocity obtained from the GPS drift.

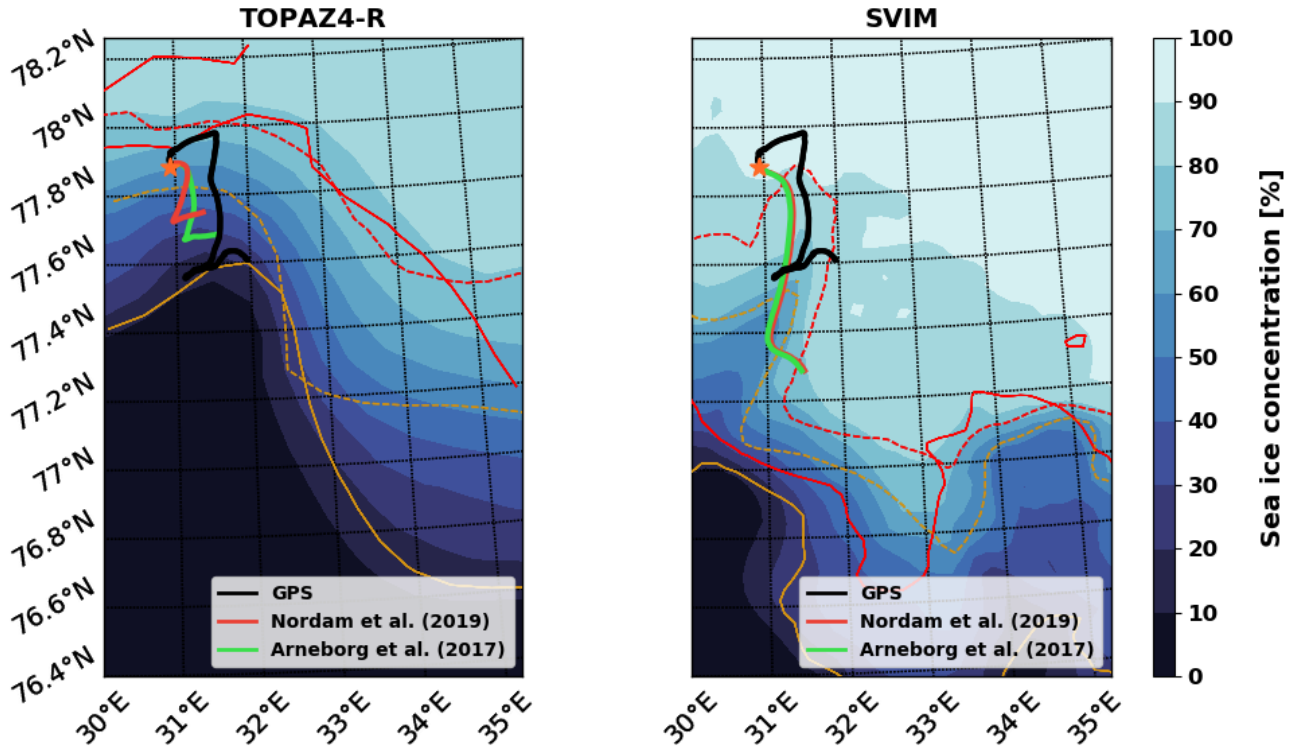

Figure 3.2: FEX09 drifter simulations forced by SVIM (left panel) and TOPAZ4-R (right panel). Observed trajectory is represented by the solid, black line and the oil-in-ice drift models by the pink (Nordam et al., 2019) and green lines (Arneborg et al., 2017). The background map represents the mean sea ice concentration ($\bar{C}$) for the period of the field experiment of each ice-ocean model. The thinner, red lines show where $\bar{C}$ = 80% in the first (solid) and last (dashed) days. The yellow lines represent the same, but for $\bar{C}$ = 30%.

The separation distances under Nordam et al. (2019) and Arneborg et al. (2017) approaches are, as expected from Figure 3.2, essentially the same when forced by SVIM (Figure **??**, top row). Values increased up to 40 km on the last day of simulation, twice as much as the separation distance obtained with TOPAZ4-R. In spite of that, simulations forced by the latter did not present any skill whereas $SS > 0$ was found under SVIM, although it decreased to zero in less than 12 hours.

3.0.2 Comparison of the simulated oil trajectories against the IABP and Nansen Legacy drifters

The second experiment intended to simulate the trajectories of IABP and AeN buoys deployed in the Arctic. Regarding the first, 15-day period simulations were conducted and the separation distance between observed and modeled trajectories for the 4 combinations between the oil-in-ice (Arneborg et al. (2017); Nordam et al. (2019)) and the coupled ice-ocean models (RIOPS and TOPAZ4-H) are presented in Figure 3.4. The mean separation distance (μ, black thick line) and the standard deviation (σ, grey shaded area) are also presented in the figure. The vertical, red dashed lines indicate every third day of simulation (3, 6, 9, 12 and 15) and their correspondent mean separation distance values are exhibited too.

By visually inspection of Figure 3.4, one can observe that the four combinations presented similar separation distances, especially when comparing the different oil-in-ice drift models forced by the same ice-ocean inputs. Around 90% of the values are present within the 1σ envelope. Similarly, all of the four set of simulations were unable to satisfactorily reproduce the trajectories of the same five drifters, out of the shaded area. The mean separation distances of both oil-in-ice drift models forced by TOPAZ4-H (38.428 km and 38.272 km) are smaller than when simulations were performed with RIOPS (39.430 km, 39.493 km), although rate of growth of the latter is slightly greater, 1.6 km day^{-1} and 1.4 km day^{-1}, respectively. On the 15th day of simulation, the model proposed by Arneborg et al. (2017) and forced by TOPAZ4-H presented the lowest mean separation distance (38.272 km), about just 1.2 km less than the the worst combination, which is Nordam et al. (2019) forced by RIOPS (39.430 km). For the four combinations, the separation distance increases nearly linearly in time, at a rate of approximately 100 m per hour.

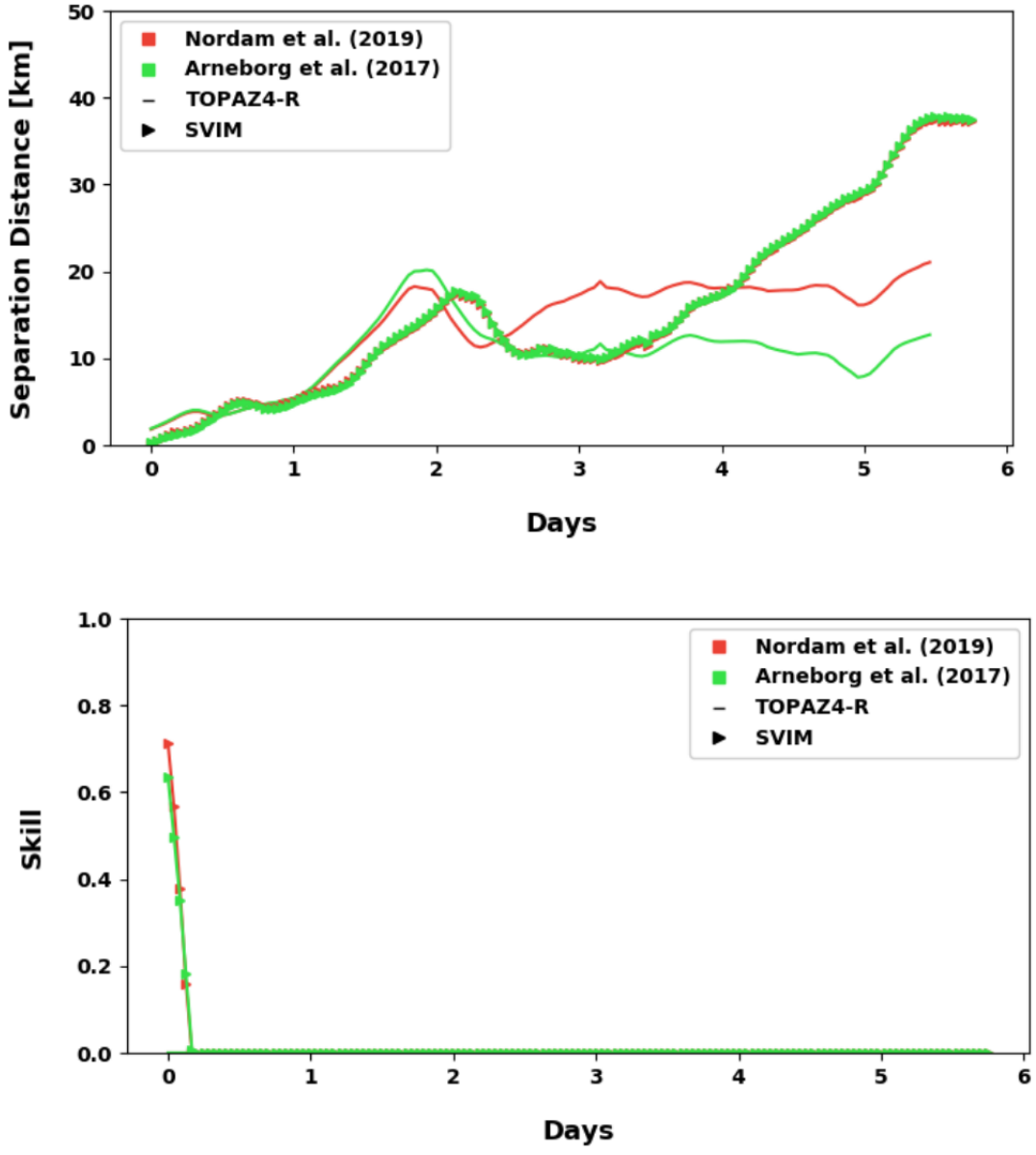

Figure 3.3: Separations distance [km] (top row) and skill values (bottom row) for the FEX09 experiment forced by SVIM (triangles) and TOPAZ4-R (solid line) under Nordam et al. (2019) (pink) and Arneborg et al. (2017) (green) approaches.

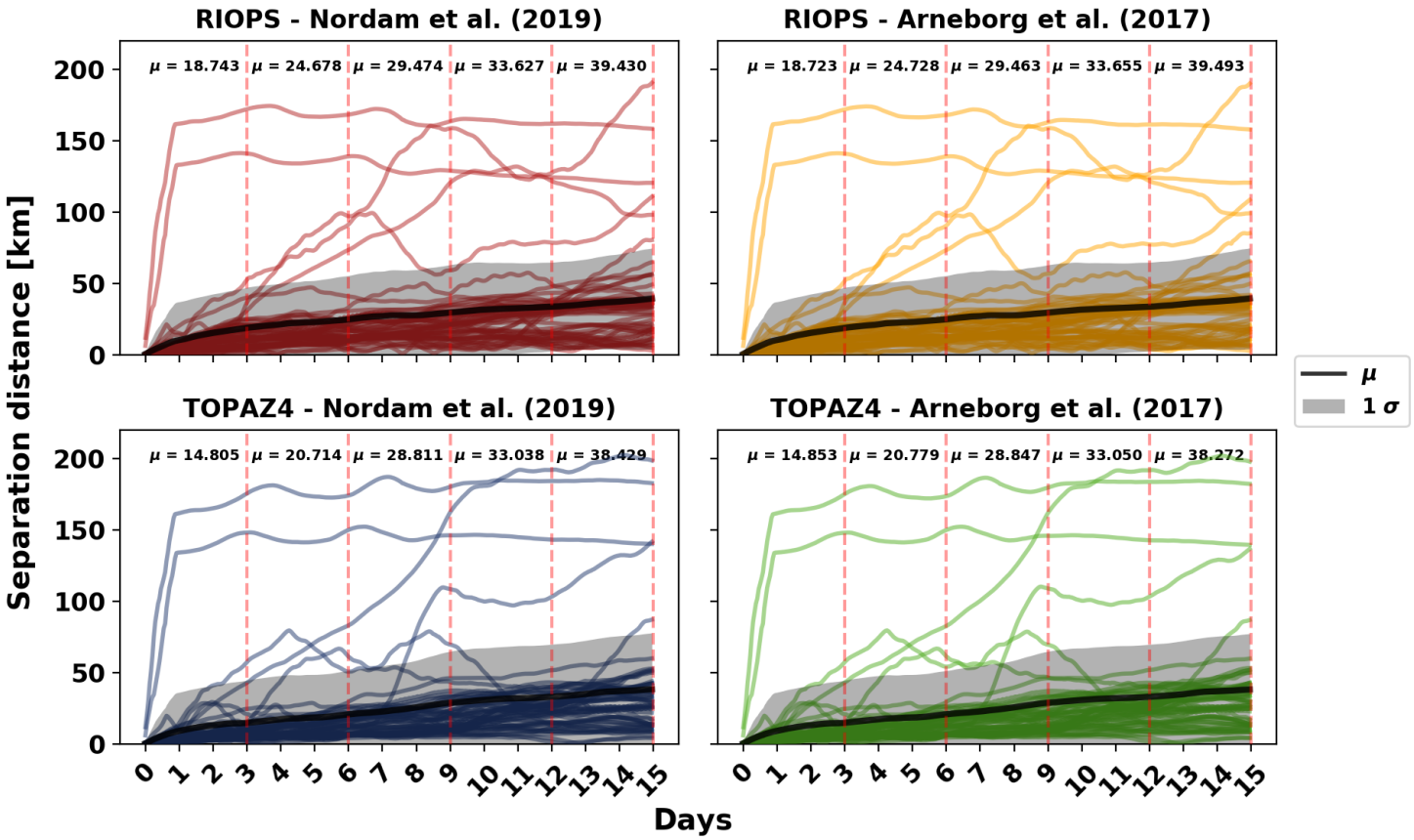

Figure 3.4: Separation distance [km] for the 15-day period runs of IABP buoys simulated by the two oil-in-ice drift models (Nordam et al. (2019) - left column; Arneborg et al. (2017) - right column) and forced by RIOPS (top row) and TOPAZ4-H (bottom row). The mean separation distance (μ) is represented by the thick black line and the standard deviation (σ) by the shaded area. Vertical, dashed lines are plotted every three days and their corresponding μ is presented on the left side.

The skills for this set of simulations, calculated by using Eq. 2.14, are presented in Figure 3.5. One can notice that the values degrade fast, reaching no skill at around 1 day after the initilization for oil-in-drift models forced by RIOPS and after about 2 days when under TOPAZ4-H forcing. Similarly to the separation distances, there is basically no difference between different oil-in-ice drift models when forced by the same ice-ocean product.

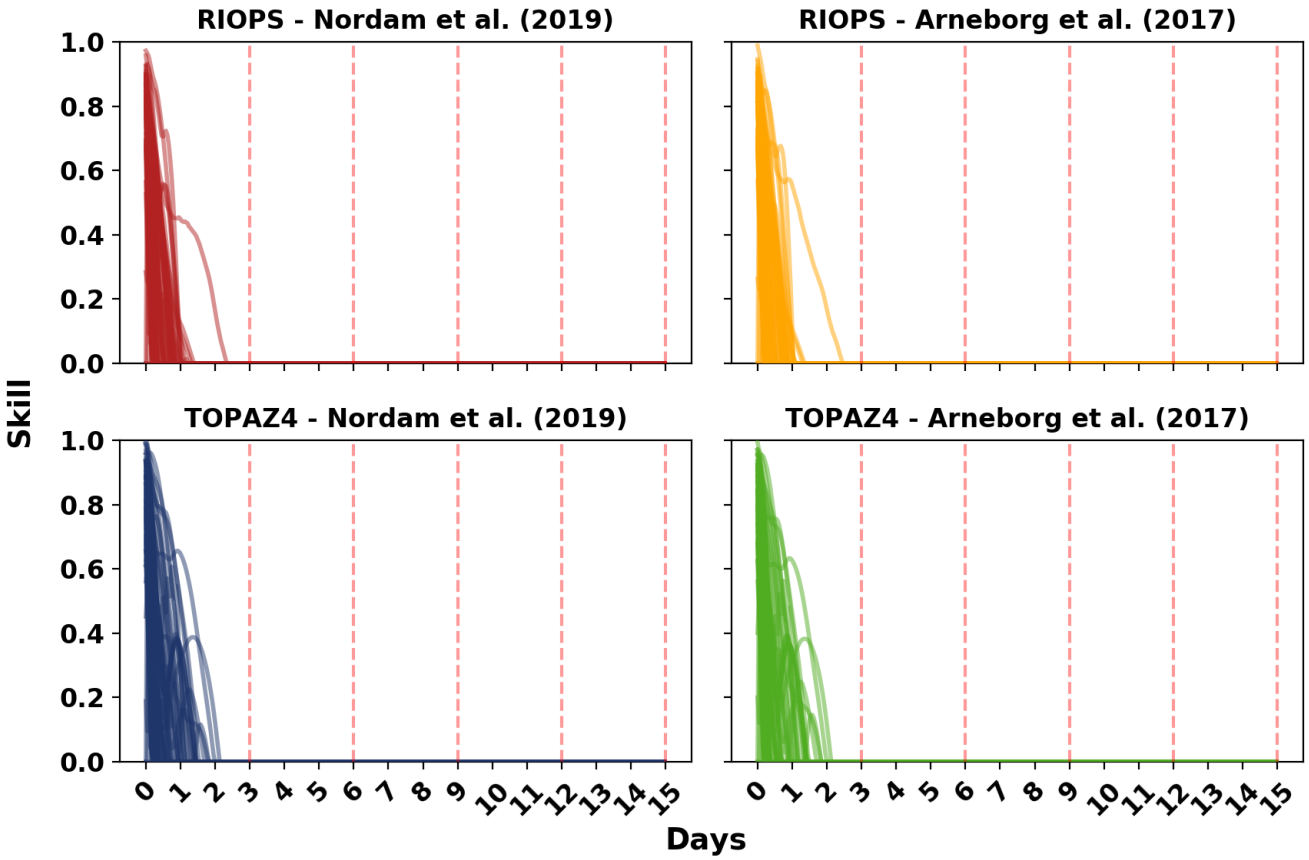

Figure 3.5: Skill values for the 15-day period runs of IABP buoys simulated by the two oil-in-ice drift models (Nordam et al. (2019) - left column; Arneborg et al. (2017) - right column) and forced by RIOPS (top row) and TOPAZ4-H (bottom row). Vertical, dashed lines are plotted every three days.

Figure 3.6 shows the separation distances for IABP buoys when simulations were re-initialized every 3 days. Note that the first three days have essentially the same mean value as in the 15-day period runs, as expected. On the subsequent segments, the mean separation distances are about 2 or 3 times smaller than for the corresponding periods in the longer simulations. Similarly to the results shown in Figure 3.4, the two oil-in-ice drift models forced by the same ice-ocean output presented fairly comparable performances, distinguishable only at the second decimal place.

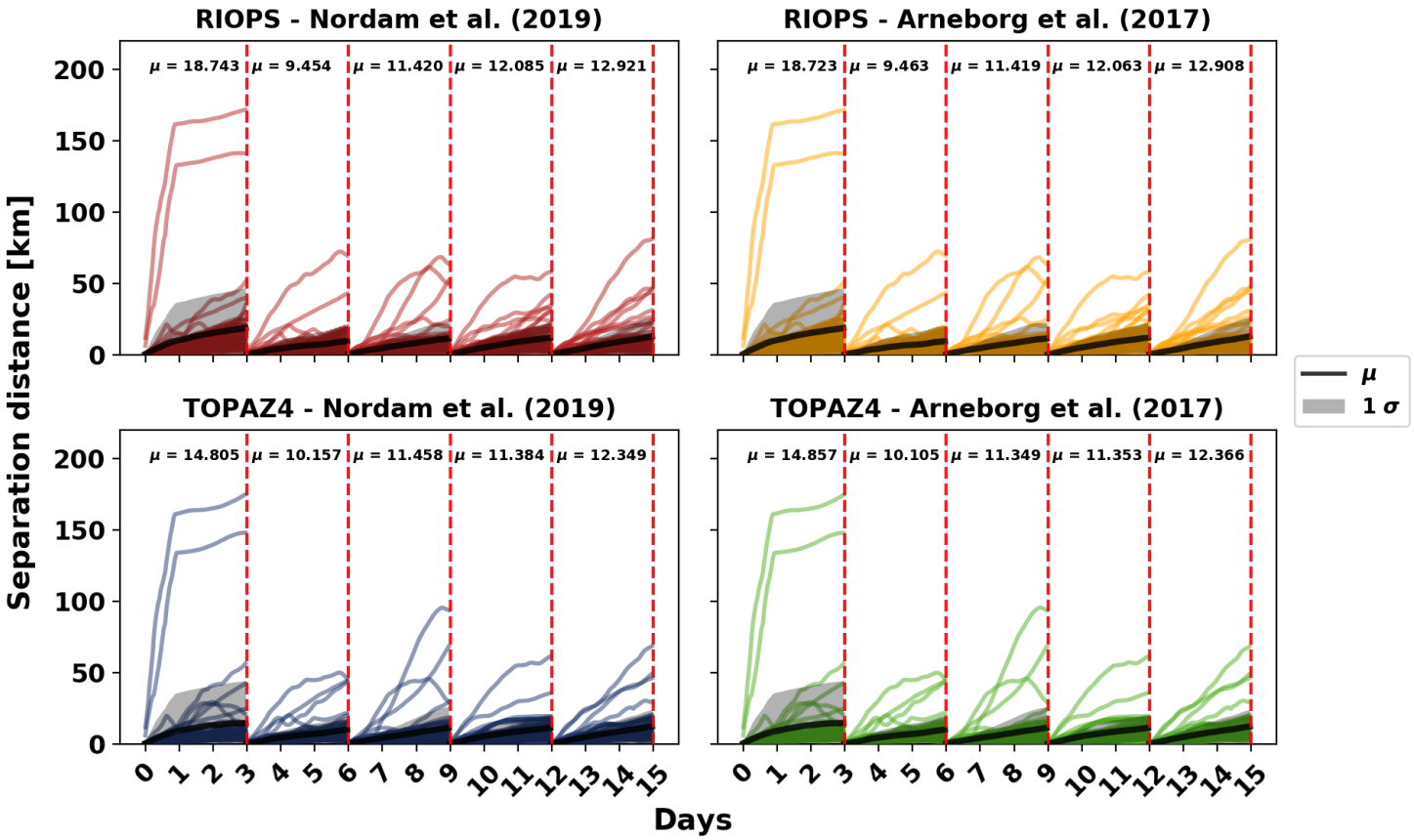

Figure 3.6: Separation distance [km] for the 3-day period re-initialized runs of IABP buoys simulated by the two oil-in-ice drift models (Nordam et al. (2019) - left column; Arneborg et al. (2017) - right column) and forced by RIOPS (top row) and TOPAZ4-H (bottom row). The mean separation distance (μ) is represented by the thick black line and the standard deviation (σ) by the shaded area. Vertical, dashed lines are plotted every three days and their correspondent μ is presented on left side.

As in the 15-day period runs, the skill values found for the re-initialized simulations are in general slightly better when models are forced by TOPAZ4-H than by RIOPS (Figure 3.7). No skill was found after 1 day of simulation when RIOPS was used whereas it extended to 2 days when the simulations were performed with TOPAZ4-H. Notice that the same drifters poorly represented in the 15-day period runs did not improve even when the simulations were re-initialized.

Regarding the four drifters deployed during the AeN cruise, the simulations had to be shortened due to beacons' shorter working period (between 7 and 12 days) compared to IABP buoys (15 days). In a similar way, the runs were also performed in a continuous and re-initialization way. Concerning the first, Figure 3.8 shows the modeled trajectories (first row), the separation distances (km, second row) and the skill (third row) obtained for the drifters when forced by RIOPS (left column) and TOPAZ4-H (right column).

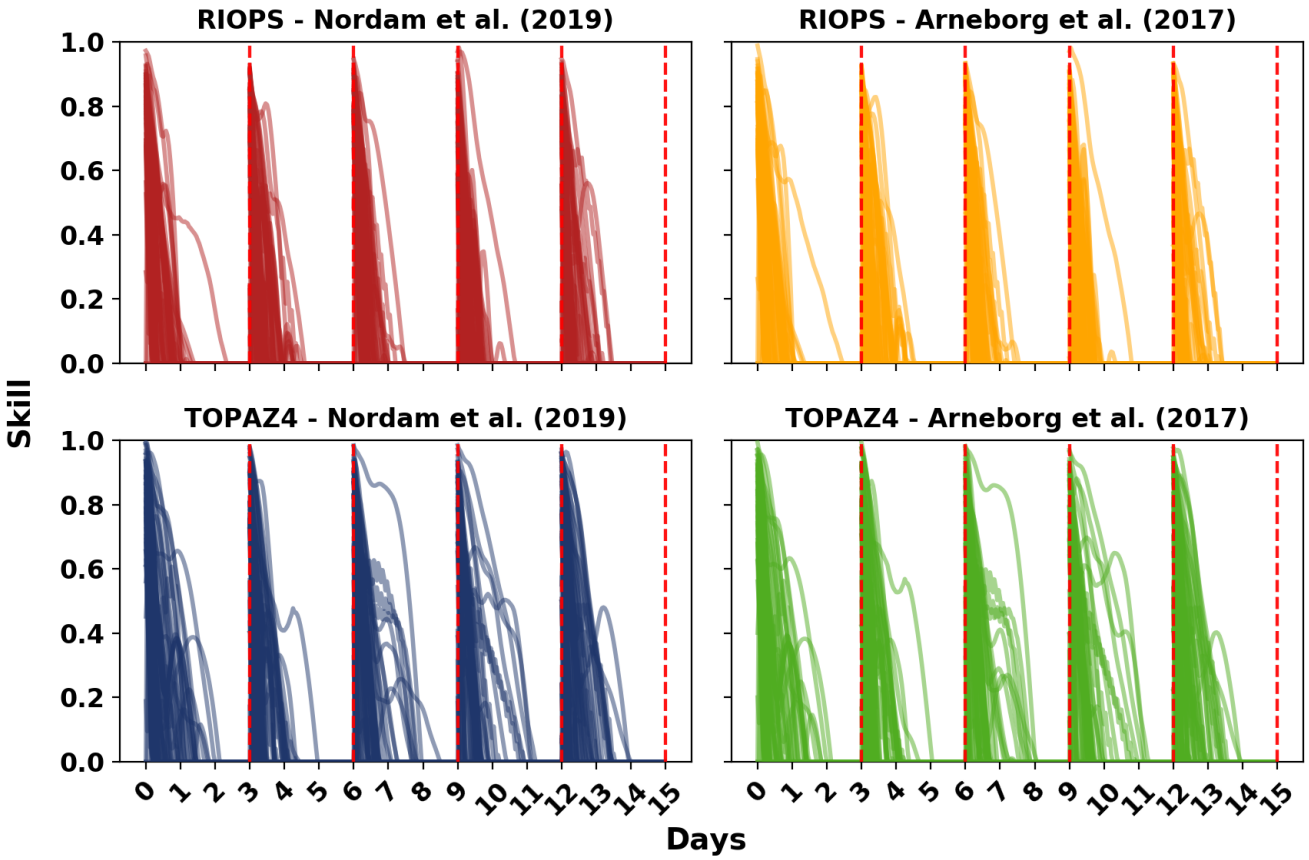

Figure 3.7: Skill values for the 3-day period re-initialized runs of IABP buoys simulated by the two oil-in-ice drift models (Nordam et al. (2019) - left column; Arneborg et al. (2017) - right column) and forced by RIOPS (top row) and TOPAZ4-H (bottom row).

The trajectory maps (Figure 3.8, top row) indicate that observed drift patterns (coloured, marked lines) are in general poorly represented by the drift models (Nordam et al. (2019) - pink; Arneborg et al. (2017) - lime green). Apart from beacon 14438 and 14435 forced by RIOPS under Nordam et al. (2019) approach, particles seems to have drifted westwards less than the observed trajectories although their shape are somehow similar. One can also notice that the eastward shift in the longer drifts (14435 and 14437) was not satisfactorily represented by the models. Moreover, with the exception of beacon 14438, the cloud of particles under Arneborg et al. (2017) approach presented an apparent higher extent of dispersion whereas particles ruled by Nordam et al. (2019) model drifted more cohesively.

The separation distances seem to have increased almost linearly in the first four days, having reached around 18 km on the third day. After that, the values corresponding to beacons 14437 and 14432 sharpened their trend and increased from 30 km to about 100 km in four days (4th to 8th day). Notwithstanding their change, the separation distances related to beacon 14435 apparently grew at constant rate throughout the simulation.

The skill values (bottom row, Figure 3.8) indicated slightly better results towards simulations forced by TOPAZ4-R. Regarding the latter, from the eight simulations, 5 of them presented skill values higher than 0 beyond the 4th day of simulation, whereas only one (beacon 14435, under Nordam et al. (2019) approach) extended for more than four days with $SS > 0$ in the runs forced by RIOPS. The skill characteristics relative to each buoy are not the same for RIOPS and TOPAZ4-H. For example, while beacons 14432 (green) and 14437 (red) have the sharpest decay under the first forcing, reaching the no-skill level before 3 days, the same beacons last the longest (up to 6 days) when TOPAZ4-H was used.

3.0.3 Stochastic simulations for a hypothetical oil spill accident in the Pechora Sea

In total, 960 simulations were performed for the hypothetical oil spill accident in the Pechora Sea. Covering the period between 1998 - 2017 (March - May), 96000 particles were released and tracked for 10 days. It is presented in Figure 3.9 the distribution of particles (24000) at the last time step of the simulations. Similarly to the previous results, the choice of the oil-in-ice model seems to be a minor constraint in 2D oil drift modeling in the presence of sea ice.

This experiment highlighted how distinct ice-ocean products provide different outputs. Simulations forced by SVIM presented a larger zonal distribution, extending from 42°E to 57°E, but limited within the meridional band between 70°N and 73°N. Conversely, when forced by TOPAZ4-R, particles covered a greater latitudinal extension, reaching the Kolguyev Island at 69°N and beyond 73°N, but bounded within 44°W and 52°W. The estimated area covered by the particles was larger in TOPAZ4-R simulations (89230 km^2; 81429 km^2) than in SVIM (68808 km^2; 80592 km^2), for Nordam et al. (2019); Arneborg et al. (2017), respectively. Please check Appendix A for further explanation regarding the surface area estimation.

Since the spatial distributions of particles forced by the same input are remarkably similar (Figure 3.9), only results related to the Nordam et al. (2019) approach are shown in Figure 3.10, with results associated to SVIM and TOPAZ4-R on the left and right columns, respectively. The top-row shows the relationship between the yearly-averaged distance traveled by the cloud of particles barycenter (km) and the associated mean sea ice concentration (%). The colored scatter represents the years of the period of interest (1998 - 2017) and the adjusted linear regression is depicted by the solid red line. The adjusted linear regression indicated a negative relation between the variables, with a slope (correlation) of -1.41 km/% (-0.90) for SVIM and -1.24 km/% (-0.76) for TOPAZ4-R. Put in words, low sea ice concentration values allow slicks to drift further away from their releasing point.

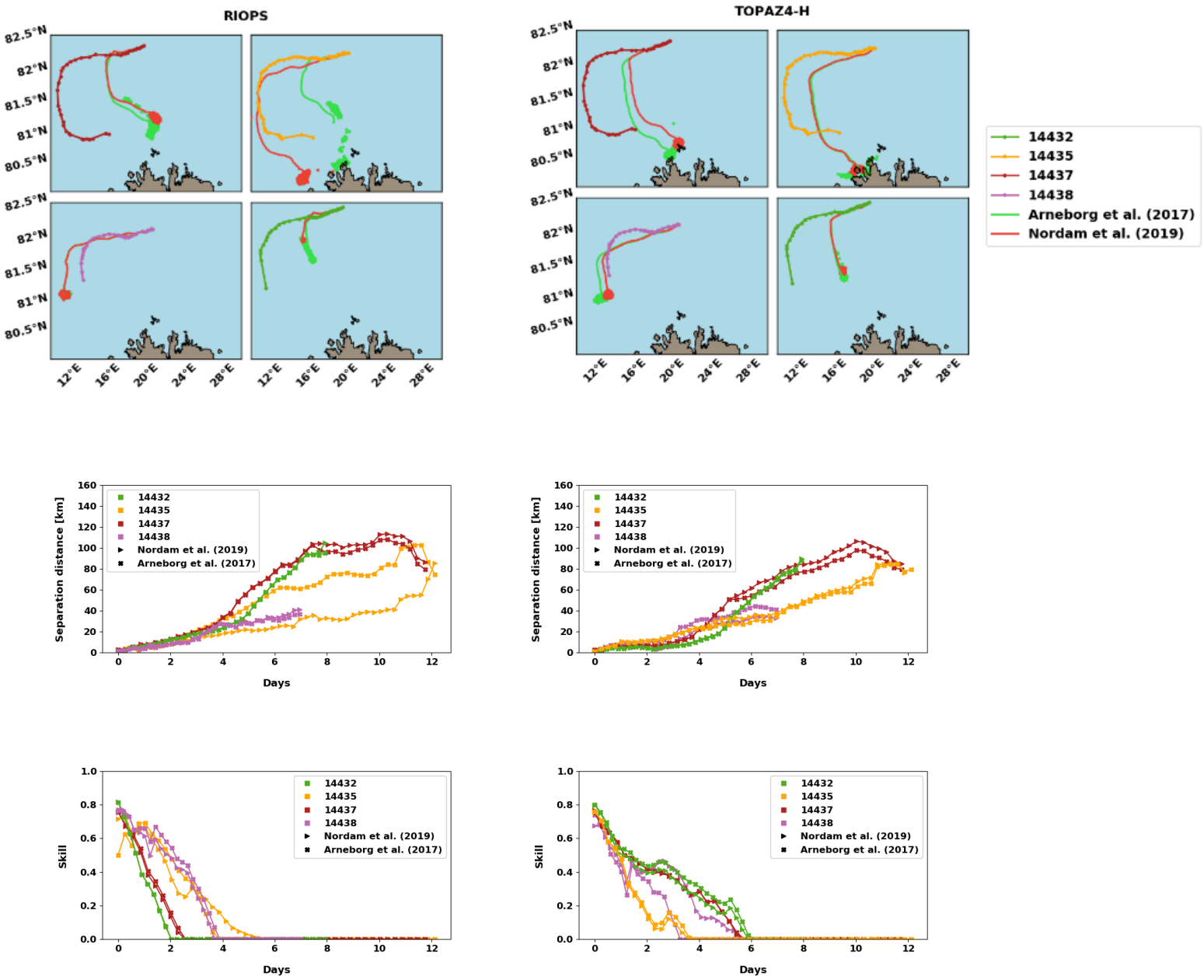

Figure 3.8: Simulated (solid lines) and observed (with markers) trajectories (top row), separation distance [km] (mid row) and skill values (bottom row) for the AeN drifters forced by RIOPS (left column) and TOPAZ4-H (right column). Nordam et al. (2019) (Arneborg et al. (2017)) oil-in-ice drift approach is represented by the pink (green) solid line in the trajectory maps and by the square (triangles) markers in the second and third row. Solid colors represent each of the four drifters, as indicated in the legend.

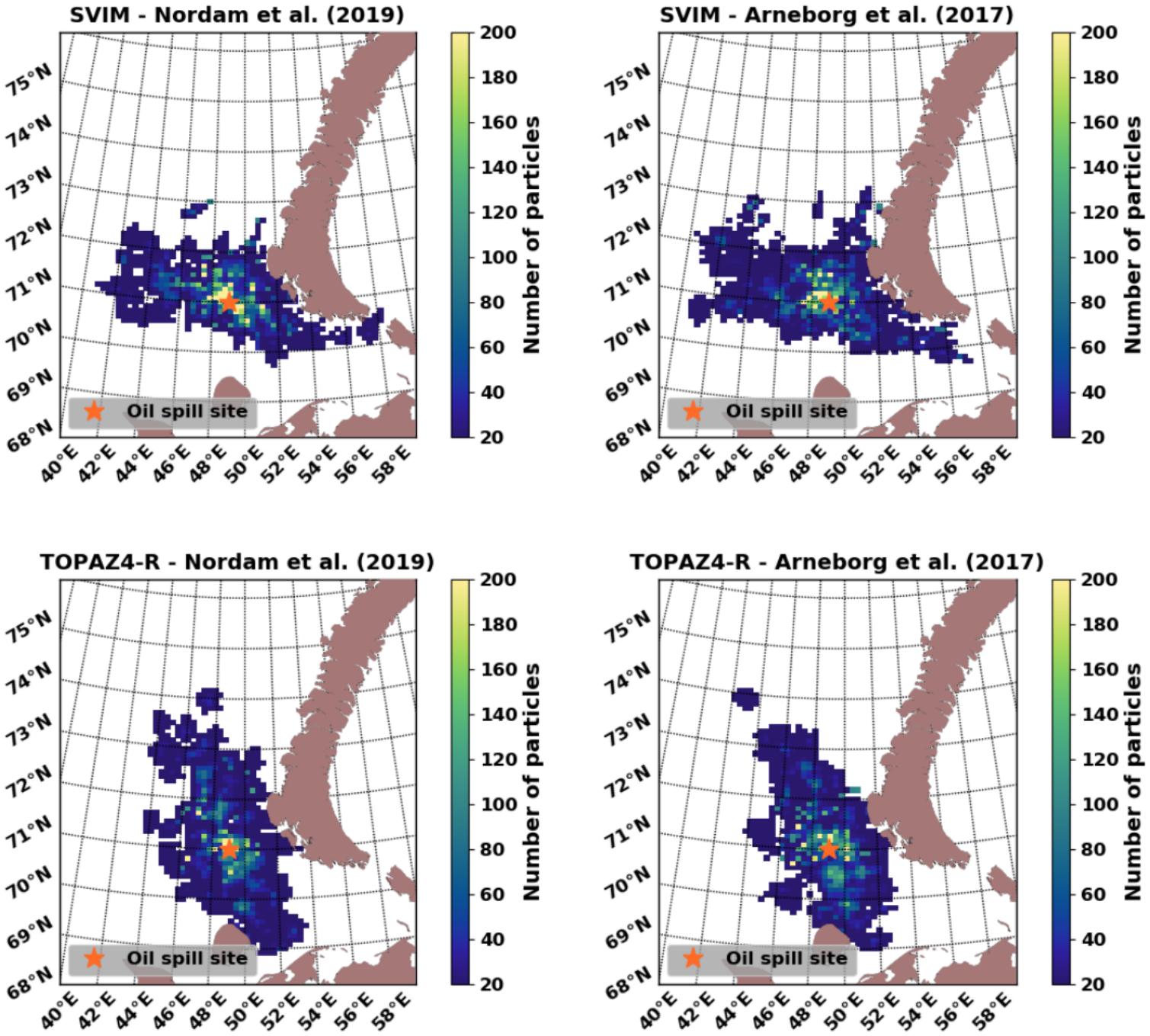

Figure 3.9: Horizontal concentration maps (number of particles) at the last time-step for stochastic oil spill simulations after 10 days summed over the 960 simulations. Forcings are displayed in the rows (SVIM - top; TOPAZ4-R - bottom) and oil-in-ice models in the columns (Nordam et al. (2019) - left; Arneborg et al. (2017) - right).

The mid-row in Figure 3.9 exhibits the intra-annual variability of sea ice concentration stored by the virtual particles. The values indicated a shift from high (> 90%, 1998 and 1999) to low sea ice concentration (< 30%, 2011 - 2017) when SVIM was used (Figure 3.10). The large

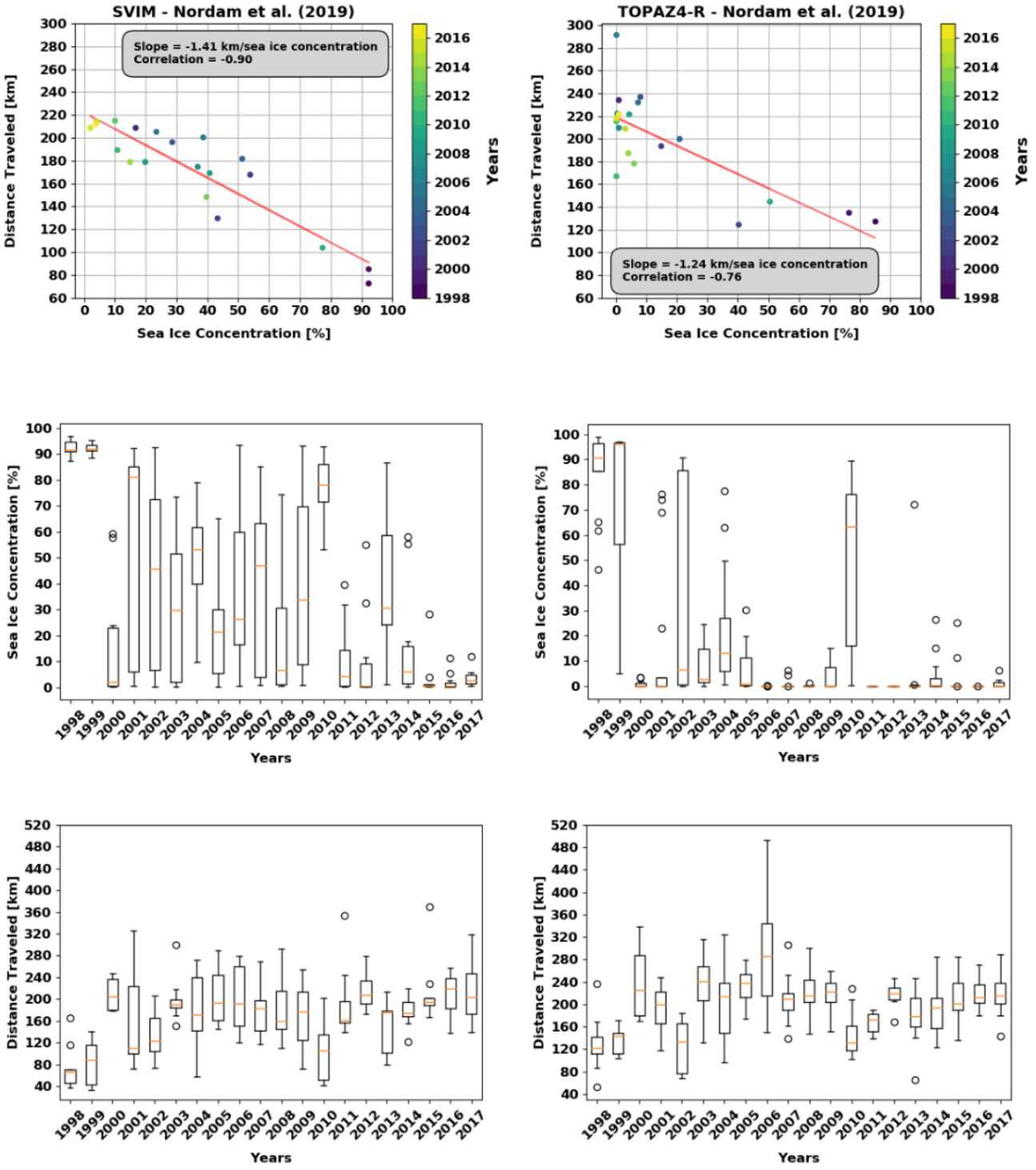

Figure 3.10: Correlation between yearly averaged sea ice concentration [%] and distance traveled [km] (top row), yearly distribution of sea ice concentration [%] (mid row) and distance traveled [%] for the 240 simulations under Nordam et al. (2019) oil-in-ice approach forced by SVIM (left column) and TOPAZ4-R (right column). The orange line in the boxplots represent the median.

interquartile range between these two periods (2000 - 2010) might represent the transition of the sea ice concentration field, marked by high variability. This is not however observed in the simulations forced by TOPAZ4-R, in which low values were consistently present since 2001.

As mentioned previously, the distance traveled by the particles and the sea ice concentration are statistically related and since the latter was generally lower in the TOPAZ4-R simulations, one could also expect that oil slicks would drift further away from the releasing point when forced by this ice-ocean inputs. In alignment with these findings, Figure 3.10 (bottom row) exhibits the intra-anunual variability of distance traveled by particles over the considered period and the results indicate that particles traveled about 20% more under TOPAZ4-R forcing. Despite the difference in magnitude, the interannual variability is similar between the two outcomes, indicating that the wind forcing might be common factor modulating the drifts.

Chapter 4

Discussion

In this study, two oil-in-ice drift models proposed by Nordam et al. (2019) and Arneborg et al. (2017) were implemented in OpenDrift (Dagestad et al., 2018), an open-source Lagrangian framework developed and maintained by the Norwegian Meteorological Institute. These two different approaches were assessed through three set of simulations: a real oil-in-ice field experiment, drifters deployed in the ice pack and in the marginal ice zone and a hypothetical oil spill in the Pechora Sea.

The first experiment had as main goal the comparison between the trajectory of virtual elements forced by a reanalysis (TOPAZ4-R) and a hindcast product (SVIM) against the trajectory of an oil spill field experiment done in the Barents Sea marginal ice zone in 2009 (Faksness et al., 2010, 2011). The first result, shown in Figure 3.1 and which the observed trajectory was simulated by using the velocity values derived from itself, had as main purpose the reproduction of the findings from Nordam et al. (2019) (see their Figure 5, left panel). Although this simulation does not provide any new insight, and actually might be seen as meaningless in terms of numerical modeling, it certified that results obtained here with OpenDrift converge to the outcomes found by the researchers.

Nonetheless, differently from Nordam et al. (2019) that reproduced relatively well the controlled spill trajectory by using another ice-ocean coupled model (SINMOD), the results presented in Figure 3.1 indicated that TOPAZ4-R and SVIM were not able to accurately simulate the mean displacement of the oil slick. Other researches (e.g French-McCay et al., 2018; Babaei and Watson, 2020) found similar results and they pointed out that discrepancies between the modeled and observed sea ice concentration field might explain the bad performance. The authors changed the spill location to satisfy the sea ice concentration conditions observed during the field experiment, resulting in skill improvements. These observations highlight that oil-in-ice models, like the ones evaluated in this work, are capable of reproduce reasonably well the drift of oil in the presence of sea ice given accurate inputs.

Faksness et al. (2011) report that the sea ice concentration during the FEX09 was around 70%-80%, whilst the values provided by TOPAZ4-R and SVIM varied between 25%-70% and 85%-92%, respectively. Since C values were larger than 80% throughout the SVIM simulations, sea ice velocities were the only forcing and hence the modeled trajectories were indiscernible (see Figure 3.2, right panel). Conversely, particles were forced by both sea water and ice velocities at different proportions with TOPAZ4-R and the trajectories under Nordam et al. (2019) and Arneborg et al. (2017) approaches were made perceivable. Despite the finer horizontal resolution, SVIM did not provide better results.

For the simulations evaluated against the drifters from the IABP program (Figure 3.4 to Figure 3.6), TOPAZ4-H provided slightly better results than RIOPS in terms of mean separation distance and skill values, but the oil-in-ice drift models responded essentially the same under a same forcing. The latter outcome was somehow expected since the main difference between the two oil-in-ice drift models materialize in transition zone $30\% < C < 80\%$. Nonetheless, the results obtained for the simulations conducted in the Barents Sea marginal ice zone for the AeN drifters also indicated that the choice of the oil-in-ice drift approach might be less relevant for 2D simulations than the considered forcing. Zhang et al. (2020) used two drift models forced by a series of multi-source datasets to reproduce the observed trajectory of drifters in the South Chine Sea in ice free conditions. Their observations also revealed that the influence of the ocean forcing field plays the dominant role on the reproduction of trajectories in the region, overcoming the influence of the chosen drift model.

RIOPS seems to have provided slightly better simulations than TOPAZ4-H with respect to the separation distance only for beacons 14438 and 14435 when under Nordam et al. (2019) approach (second row, Figure 3.8). Apart from that, RIOPS did not provide better results neither in the ice pack nor in the marginal ice zone despite its finer horizontal resolution. These results coincide with the observations made by de Vos et al. (2021) that increasing grid resolution is not a guarantee of a better performance if sea ice parameterizations are not improved. Similar findings were found for drifters deployed in the North Sea and Norwegian Sea, where the absence of improvement was related to the ill description of mesoscale features by the non-assimilative high resolution ($\approx$ 2.4 km) regional model NorShelf (Dagestad and Röhrs, 2019).

It is not obvious why the finer resolution models (SVIM and RIOPS) did not present better results in comparison to the TOPAZ4 products. In general, three forces dominate the momentum equation of sea ice, namely the atmospheric and water stress and the internal forces in the ice (Tsamados et al., 2014). The latter relates the stress caused by sea ice interactions with the deformation of the ice cover (strain) and it is still considered one of the points that limit the success of ice models despite the variety of approaches Feltham (2008). In this sense, one

potential source of the lack of skill improvement is the EVP sea ice rheology scheme, used by the model products considered in this study.

The EVP rheology is currently the most commonly used scheme in operational and global climate models that include sea ice, especially due to its computational efficiency and relatively accurate description of the main, large scale (> 100 km) sea ice drift features (*e.g.* Beaufort gyre) (Dansereau et al., 2016). On the other hand, it seems to not satisfactorily reproduce properties at fine scales (Dansereau et al., 2016), which are the most relevant for oil drift operations. By simulating IABP drifter trajectories using the free drift model and neXtSIM (neXt generation Sea Ice Model) (Rampal et al., 2016), a dynamic-thermodynamic sea ice model based on Elasto-Brittle (EB) rheology, Rabatel et al. (2018) highlighted how not considering the sea ice strength and interactions (free drift) can rapidly degrade forecasting skills in winter, when the ice pack is more compact. The authors found ensemble mean position errors of 7.5 km for 3-day drift simulations in winter.

French-McCay et al. (2018) also used IABP buoys to validate oil-in-ice drift simulations and their findings indicate improvements in the skill when the EB rheology is applied instead of EVP. French-McCay et al. (2018) found mean separation distances of about 21 km, 35 km and 45 km on the 5h, 10th and 15th day of simulation for ice-ocean models using the EVP whereas it was found in this work d values of about 22 km, 29 km and 39 km for the same correspondent days of simulation. According to the authors, the separation distance decreased to 14 km, 21 km and 26 km when neXtSIM was used.

Although such evidences suggest that the used rheology scheme might be a limiting factor in modeling oil drift in the presence of sea ice, the wind forcing seems to be the primary source of uncertainty even in the ice pack (Cheng et al., 2020). The atmosphere-ice and ice-ocean stresses are proportional to drag coefficients and consequently the accuracy of the ice velocity models greatly depends on how drag coefficients are parameterized (Chikhar et al., 2019). These are strongly related to the boundary layer stability, enhanced (reduced) in unstable (stable) conditions, but the sea ice roughness and its topography might also be considered in the form of frictional skin and form drag components, respectively (Tsamados et al., 2014; Lüpkes and Gryanik, 2015; Martin et al., 2016; Petty et al., 2017). None of the ice-ocean models used here adopts the ice topography dependent form drag coefficient, considered to be more physically realistic (Chikhar et al., 2019).

Due to its proximity to open waters, drifters in the marginal ice zone can be highly influenced by oceanographic processes considered of minor importance in the ice pack. Johannessen et al. (1992) investigated the ambient noise obtained in a series of acoustic experiments conducted in the Fram Strait, East Greenland Sea and Barents Sea marginal ice zones and their findings indicated high correlation between ice motion and tidal currents. Moreover, the

tidal model used by these same authors explained more than 63% of the observed ambient noise. Modeling (*e.g.* Gjevik et al. (1994)) and field observations (Seasonal Ice Zone Experiment, 1989 - SIZEX 89) indicated tidal current with velocities up to 0.8 m s^{-1}, higher than the observed velocity of drifters released in the East Greenland Current during the same experiment (0.3 m s^{-1}). Tidal currents thus seem to be an important feature to be taken into account when modeling sea ice drift in the MIZ but although they are actually considered in RIOPS, nonetheless absent in TOPAZ4-H, such an improvement did not produce better results as well.

Beyond tidal variability, ice floes in the Barents Sea marginal ice zone might also be influenced by surface gravity waves. When traveling from the open ocean towards the MIZ, short surface gravity waves are damped by the sea ice and part of the their energy accelerates the floes through wave radiation stress convergence. Numerical studies revealed that such interactions might generate along-edge ice jets (Dai et al., 2019), similar to the ones generated by along-edge jet winds (Heorton et al., 2014). Feltham (2005) was also able to reproduce an along-edge ice jet by considering the MIZ as a granular media, pointing out that its formation arises naturally as a consequence of the granular nature of sea ice. Muench and Schumacher (1985) observed along-edge jets at speeds of 10 - 15 $^{-1}$ in the Bering Sea, well above of the 2 - 5 cm s^{-1} current speeds that typify the region under regular conditions. These submesoscale features have widths of 10-15 km (Johannessen et al., 1983) and can increase the transport of sea ice by 40% in comparison to the ice pack (Heorton et al., 2014). None of the ice-ocean models used here solve wave-ice interactions, present horizontal resolutions of at least 2 km (Heorton et al., 2014) nor treats sea ice as granular material (Feltham, 2005), thus being unable to reproduce this apparently important component of sea ice drift. In addition, the transition of the wind stress over the ice-ocean boundary in the MIZ might create ocean currents parallel to the ice edge associated to upwelling formation (Johannessen et al., 1983).

The aforementioned along-edge currents and jets might be unstable and trigger eddies formation with scales of 10 to 40 km (Johannessen et al., 1983, 1987). RIOPS, and in a lesser extent TOPAZ4-H, are theoretically able to reproduce eddies of this extent, but their eddy-permitting characteristic breaks down when the feature scales approach the Rossby radius (R), $\mathcal{O}$(R), which can be as small as 1 - 2 km in the Arctic Sakov et al. (2012). Eddies in the Arctic MIZ, and their role on reshaping the ice edge through basal melting, have been reported since the early 80's (Johannessen et al., 1987), but just recently their characteristics have been assessed by observations (Kozlov et al., 2019) and numerical experiments (Wekerle et al., 2020; Platov and Golubeva, 2020). Despite the different approaches and regions of study, their findings converge to the points that 1) cyclonic eddies are more common than anti-cyclones and 2) their mean radius is about 5 km. In addition, by conducting numerical experiments, Wang et al. (2020) suggested that grid sizes of *at least* 1 km are required

to resolve eddies in the Artic basin. It seems thus plausible that one of the sources of inaccuracies in this work is the inability of both RIOPS and TOPAZ4-R reproduce accurately mesoscale eddies in the MIZ, although improving their horizontal resolution might not be guarantee of obtaining better results (Dagestad and Röhrs, 2019).

The obtained skills for the IABP simulations degraded to 0 (no skill) between 1 and 2 days, faster than reported by French-McCay et al. (2018) that found $SS > 0$ up to 5 days. Unfortunately, the authors did not present the tolerance threshold (n in Eq. 2.14) used in their work, thus limiting a direct comparison. Since the mean separation distances found here are actually smaller than obtained by French-McCay et al. (2018), either the tolerance threshold (n) used by them is greater than 3 or the cumulative observed drift here is smaller. Since both works use data from the same region and program, although in different periods, it is likely that the observed trajectories present similar displacements.

When comparing the separation distances found in ice covered regions to the ones obtained in ice free areas, values are usually smaller in the first. For instance, it was found in this work a mean separation distance of about 22 km after 6 days of simulation (see Figure 3.4), whereas Dagestad and Röhrs (2019) obtained a comparable value after only 2 days for drifters released in the North Sea and Norwegian Sea, and Liu and Weisberg (2011) reports mean separation distances of 73 and 27 km after 2 days of simulation for drifters located in ocean interior and continental shelf in the Gulf of Mexico, respectively. Nonetheless, the observed displacement of drifters in ice free areas is larger than of buoys released in the ice pack and hence the larger separation distances are compensated by longer drifts. Conversely, in sea ice covered areas, drifters generally travel less and are not able to balance the continuous error increase.

In this sense, as one can deduce from Eq. 2.14 but also pointed out by Liu and Weisberg (2011), short observed displacements can largely increase s despite d being small, hence rapidly decreasing the skill. Using the same tolerance threshold for the simulations conducted in the ice pack (IABP) and in the marginal ice zone (AeN) seems to be unreasonable, and it might explain why skill values for the latter were superior although one can notice by visual inspection that the simulated trajectories did not reproduce accurately the observed drifts. Such an explanation might also be extended to the FEX09 simulations, in which the longer distance traveled by the particles when forced by SVIM counterbalanced the larger separation distance (see Figure 3.2.

The re-initialization of the simulations improved the skills in periods of the 15-day IABP runs which SS values > 0 were not present. Although the mean separation distances being about two to three times smaller relatively to their correspondent days in the longer simulations, the skill decay presented the same pattern throughout the re-initialization runs, not extend-

ing further than 2 days in the case of particles under TOPAZ4-H and around 1 day when forced by RIOPS. One should notice that no skill was obtained on every third day (3, 6, 9, 12 and 15) in any of the simulations. Nonetheless, since models are re-initialized more often than 3 days in operational oil spill operations, such an issue can be easily suppressed.

The last set of simulations reproduced an hypothetical oil spill in the Pechora Sea, next to the Kara Gate, in a region which the sea ice concentration has been significantly changing over the years (see Figure 2.4). By randomly selecting the initial releasing date, 240 x 4 10-day simulations between March - May (1998 - 2017) were performed. The conceptualization of this experiment was based on similar approaches conducted by Röhrs et al. (2018); Morell Villalonga et al. (2020) and it aimed the evaluation of how different ice-ocean inputs and the sea ice reduction impact oil-in-ice trajectories.

Converging to the findings presented previously, the results of this experiment also revealed that the used ice-ocean forcing is more relevant for 2D oil-in-ice modeling than the choice of the drift approach. The lower sea ice concentration present in the TOPAZ4-R (Figure 3.10, middle row) might explain the greater area extent covered by the particles, their longer displacement when compared to simulations forced by SVIM.

The hydrodynamic in the Pechora Sea is mainly controlled by the inflow of the North Cape Current (NtCC), a branch of the Norwegian Atlantic Current (NAC), and the Norwegian Coastal Current (NCC) through the so-called Barents Sea Opening, located between Norway and the Bear Island (Gammelsrød et al., 2009). Once in the Pechora Sea, NtCC is then renamed to Murmansk Current (MC) whereas the NCC to Murmansk Coastal Current (MCC) (Loeng, 1991). Flowing eastwards at first, the NtCC shifts northwards at around 45°E, running parallel to Novaya Zemlya's coastline (Wassmann et al., 2006).

Oil spill modeling studies in the Pechora Sea are still scarce despite the high traffic of tanker ships through the Kara Gate and the presence of oil exploration facilities, including the Prirazlomnaya Arctic oil terminal (69.266°N, 57.285°E). Nordam et al. (2017) simulated hypothetical spills in the Kara Gate and in the Varandey oil terminal, next to Prirazlomnaya, in the present (2009-2012) and future (2050-2053) years. The authors identified that the ice cover is extremely important on oil fate prediction, but no considerations were made regarding oil transport. This observation and the previously described ocean surface currents configuration might be an indication of the predominant role of sea currents over the sea ice drift, culminating in the general meridional displacement of particles under the TOPAZ4-R forcing.

The World Wildlife Fundation - Russia (WWF-Russia), through the Risk Informatics Research Guidance Center, conducted a series of oil spill simulations at the location of the Prirazlomnaya terminal in ice-free conditions and in the presence of sea ice. Their findings indicate

that during the former period particles are able to reach the Kolguyev Island and cross the Kara Gate, located at around 250 km and 150 km away from the spill location, respectively. Conversely, the presence of sea ice limited the oil trajectories within a radius between 50 km and 75 km, impacting only the near coastline south of the oil terminal (Informatics, 2012). This highlights that the releasing position is an important factor when modeling oil spills in the Pechora Sea.

Chapter 5

Conclusions and Recommendations for Further Work

5.1 Conclusions

The assessment of two oil-in-ice surface drift models implemented in OpenDrift, an open-source Lagrangian framework developed in Python, was conducted in this work. Proposed by Arneborg et al. (2017); Nordam et al. (2019), both models are based on the "30/80" rule-of-thumb which states that oil drifts as in open waters when the sea ice concentration $C <$ 30% and with the ice field when $C \geq 80\%$. For the intermediate values, each model presents a different transition, as shown in Subsection 2.1.3.

The oil-in-ice drift models were evaluated under three different set of simulation: (I) a field experiment in the Barents Sea marginal ice zone in 2009 (FEX09); (II) buoys from the IABP program located in the ice pack (2018 - 2019) and wave sensors also released in the Barents Sea marginal ice zone during the Arven etter Nansen (AeN) cruise in 2018 and (III) a hypothetical oil spill in the Pechora Sea, next to the Kara Gate. Due to the different periods of interest, distinct metocean forcing fields were used, namely the TOPAZ4 (12.5 km) reanalysis and SVIM hindcast (4 km) for the first and third simulations, and TOPAZ4 (12.5 km) and RIOPS (3 km) operational products for the second set of experiments. The separation distance between the observed and modeled trajectories and the skill metric proposed by Liu and Weisberg (2011) were used to evaluate the performance of the two oil-in-ice drift models and the different forcing inputs on the first and second set of simulations in experiments (I) and (II).

The results obtained in this study suggest that the two oil-in-ice models provide similar trajectories when forced by the same ice-ocean input, both in the ice pack and in the marginal

ice zone. Results from the experiments (I), FEX09, and (II), IABP and AeN, fairly agreed with previous works (e.g. Nordam et al., 2019; French-McCay et al., 2018), and this might be an indication that both drift approaches were implemented correctly. Having this said, the models are freely available for use and improvements in OpenDrift.

Results from experiments (I) and (II) also indicated the observed trajectories were not better reproduced, neither in the ice pack nor in the MIZ, when simulations were performed with the finer resolution inputs (SVIM and RIOPS, respectively). Many reasons might justify such a finding, but a quantitative evaluation of them is out of the scope of the present research and hence they are limited to speculations. In the ice pack, where the IABP buoys were released, the sea ice internal forces and wind-ice stress play a major role on the ice motion, so sensitivity studies regarding sea ice rheology parameterizations and the inclusion of the ice topography on the form drag might improve our understanding of the uncertainties present in sea ice modeling. The closeness to the open ocean and the sharp wind drag coefficient transition result in the formation of features not present in the ice pack and rarely solved by ice-ocean models. RIOPS does include tidal motions, but this improvement in comparison to TOPAZ4-R did not provide better results as well. In addition, none of them solve wave-ice interactions, considered as a key factor in the MIZ. Finally, the horizontal resolutions of the ice-ocean models used here seems to not be fine enough to properly reproduce mesoscale motions such as along-edge ice jets and eddies, natural features present in the region.

The separation distances for the IABP experiment are in agreement with previous researches (e.g. French-McCay et al., 2018), with a mean value around 38.5 km on the 15th day of simulation and decreasing to less than one third of this when the simulations were re-initialized every three days. No skill was found beyond the second (first) day of simulation when TOPAZ4-H (RIOPS) was used, indicating that the model re-initialization must done in a shorter period of time in real oil spill operations to avoid error exacerbation.

In case of the AeN simulations, the separation distances were higher (about 100 km on the 12th day of simulation) despite their shorter life span. The skill values extended up for 6 days, suggesting better agreements between observed and modeled trajectories. Nonetheless, this apparent better performance might be actually a bias associated to the skill formulation itself, more specifically between the arbitrary choice of the threshold parameter n and the distance traveled by the observed drifters. Since the latter is associated to the sea ice concentration, the threshold parameter should be carefully chosen to accommodate the different ice conditions (*e.g.* ice pack or open water) that drifters might be subject to. In addition, assessing objective approaches, such as the Circle Assessment method (Furnans et al., 2005) or the Willmott skill score (Willmott, 1981), might provide valuable insights on the trajectory modeling evaluation field.

The hypothetical oil spill in the Pechora Sea revealed how ice-ocean inputs, in this case SVIM and TOPAZ4-R, produced distinct features of particle trajectories. The sea ice concentration field dictates the spread, the predominant direction of trajectories and the distance traveled by the cloud of particles, as revealed by Figure 3.9 and Figure 3.10. The slope (correlation) between sea ice concentration and the distance traveled by oil slicks were presented here for the first time and they are statistically significant for both SVIM, -1.41 km/% (-0.90), and TOPAZ4-R, -1.24 km/% (-0.76).

So far, only one study used climate simulations (Nordam et al., 2017) to investigate the change of oil trajectories due to the Arctic sea ice reduction. Their results are however limited to 8 years and hence a natural step would be the extension of their work to cover a longer period. Climate simulations and oil spill modeling are intrinsically surrounded by uncertainties, so a set of ensemble simulations might be a valuable approach to the problem. The Community Earth System Model Large Ensemble project (CESM-LE) provides 40 members of fully-coupled simulations for the period 1920-2100. This dataset was used in a series of publications (e.g. Årthun et al., 2019) and it might be a potential forcing for the simulations. CESM-LE has a horizontal resolution of 1°x1°, and hence a downscaling procedure might be required for oil modeling purposes.

We have demonstrated here that the Lagrangian models implemented in the open-source model framework OpenDrift (Dagestad et al., 2018) were able to reproduce the drift of oil in the presence of sea ice. Stochastic simulations are a valuable tool in Environmental Risk Analysis, providing information to be incorporated into Net Environmental Benefit Analysis, to ultimately support managers on the choice of the most efficient oil spill response techniques for mitigation of environmental impacts caused by oil spills. End-to-end ecosystem models have been coupled to oil model outputs to quantitatively estimate the impacts of oil in marine ecosystems (e.g. Ainswort et al., 2018). Currently, there is no similar system for the Barents Sea, but the region counts with an end-to-end ecosystem model called NoBa (e.g. Hansen et al., 2016) and a suggestion for further studies would be coupling it with OpenDrift outputs.

Although the main goal here was the evaluation of oil-in-ice drift models, part of the limitations of this work resides on the oil considerations itself, since only one type of oil was used, no weathering processes were taken into account and no vertical displacements were allowed. All of these factors directly impact the horizontal drift of an oil slick and should hence be investigated in further studies. Lastly, the scarceness of available drifter data in the marginal ice zone constrains robust analysis and thus an interesting aspect to look at would be to use a larger dataset to check if the findings presented in this research are still valid.

References

[1] Afenyo, M., B. Veitch, and F. Khan (2016). A state-of-the-art review of fate and transport of oil spills in open and ice-covered water. *Ocean Engineering 119*, 233 – 248.

[2] Ainswort, C., C. Paris, N. Perlin, L. Dornberger, W. I. Patterson, E. Chancellor, S. Murawski, D. Hollander, K. Daly, I. Romero, F. Coleman, and H. Perryman (2018). Impacts of the deepwater horizon oil spill evaluated using an end-to-end ecosystem model. *PLoS ONE 13*(1: e0190840), 1 – 21.

[3] Ambjorn, C. (2008). Seatrack web forecasts and backtracking of oil spills - an efficient tool to find illegal spills using ais. In *2008 IEEE/OES US/EU-Baltic International Symposium*, pp. 1–9.

[4] Androulidakis, Y., V. Kourafalou, L. Hole, M. Le Hénaff, and H. Kang (2020). Pathways of oil spills from potential cuban offshore exploration: Influence of ocean circulation. *Journal of Marine Science and Engineering 8*(7), 1–32.

[5] Arneborg, L., A. Höglund, L. Axell, M. Lensu, O. Liungman, and J. Mattsson (2017). Oil drift modeling in pack ice – sensitivity to oil-in-ice parameters. *Ocean Engineering 144*, 340 – 350.

[6] Årthun, M., T. Eldevik, and L. H. Smedsrud (2019). The role of atlantic heat transport in future arctic winter sea ice loss. *Journal of Climate 32*(11), 3327 – 3341.

[7] Babaei, H. and D. Watson (2020). A preliminary computational surface oil spill trajectory model for ice-covered waters and its validation with two oil spill events: A field experiment in the barents sea and an accidental spill in the gulf of finland. *Marine Pollution Bulletin 161*, 111786.

[8] Bambulyak, A., A. Sydnes, and M. Sydnes (2015). Oil-spill response in the russian arctic. In L. Jensen and G. Hønneland (Eds.), *2008 IEEE/OES US/EU-Baltic International Symposium*, pp. 66–86. Edward Elgar.

[9] Beegle-Krause, C., T. Nordam, M. Reed, and R. Daae ("2017"). "state-of-the-art oil spill trajectory prediction in ice infested waters: A journey from high resolution arctic-wide satellite data to advanced oil spill trajectory modeling-what you need to know". *"International Oil Spill Conference Proceedings" "1"*, "1507 – 1522".

[10] Bender, M. L., J. Giebichenstein, R. N. Teisrud, J. Laurent, M. Frantzen, J. P. Meador, L. Sørensen, B. H. Hansen, H. C. Reinardy, B. Laurel, et al. (2021). Combined effects of crude oil exposure and warming on eggs and larvae of an arctic forage fish. *Scientific reports 11*(1), 1–17.

[11] Bennett, A. (2006). *Lagrangian kinematics*, pp. 5–15. Cambridge Monographs on Mechanics. Cambridge University Press.

[12] Brandvik, P., P. Daling, and J. Myrhaug (2009, Jul). Mapping weathering properties as a function of ice conditions : a combined approach using a flume basin verified by large-scale field experiments.

[13] British Petroleum (2019). Statistical review of world energy, 68th edition. Technical report.

[14] Canada's Oil & Natural Gas Producers (2018). 2018 Economic Report Series; Canada's Role in the World's Future Energy Mix. https://www.capp.ca/wp-content/uploads/2019/11/2018_Economic_Report_Series_Canada_s_Role_in_the_World_s_Future_Energy_Mix-317291.pdf. [Online; accessed 19 October 2020].

[15] Carpenter, A. (2019). Oil pollution in the north sea: the impact of governance measures on oil pollution over several decades. *Hydrobiologia 845*, 109–127.

[16] Cheng, S., A. Aydoğdu, P. Rampal, A. Carrassi, and L. Bertino (2020). Probabilistic forecasts of sea ice trajectories in the arctic: Impact of uncertainties in surface wind and ice cohesion. *Oceans 1*(4), 326–342.

[17] Chikhar, K., J.-F. Lemieux, F. Dupont, F. Roy, G. C. Smith, M. Brady, S. E. L. Howell, and R. Beaini (2019). Sensitivity of ice drift to form drag and ice strength parameterization in a coupled ice–ocean model. *Atmosphere-Ocean 57*(5), 329–349.

[18] Commission, O. (2017). Ospar report on discharges, spills and emissions from offshore oil and gas installations in 2017.

[19] Copernicus Marine Environment Monitoring Service (2018). Ocean Products. https://resources.marine.copernicus.eu/?option=com_csw&task=results. [Online; accessed 19 November 2020].

[20] Corporation, V. (2019, September). Vn100 product specification. https://www.vectornav.com/docs/default-source/documentation/vn-100-documentation/PB-12-0002.pdf?sfvrsn=9f9fe6b9_18, accessed 20/12/18.

[21] Cox, J. C. and L. A. Schultz (1981). The containment of oil spilled under rough ice. *International Oil Spill Conference Proceedings 1981*(1), 203–208.

[22] Dagestad, K.-F. and J. Röhrs (2019). Prediction of ocean surface trajectories using satellite derived vs. modeled ocean currents. *Remote Sensing of Environment 223*, 130–142.

[23] Dagestad, K.-F., J. Röhrs, Ø. Breivik, and B. Ådlandsvik (2018). Opendrift v1.0: a generic framework for trajectory modelling. *Geoscientific Model Development 11*(4), 1405–1420.

[24] Dai, H.-J., J. C. McWilliams, and J.-H. Liang (2019). Wave-driven mesoscale currents in a marginal ice zone. *Ocean Modelling 134*, 1–17.

[25] Dansereau, V., J. Weiss, P. Saramito, and P. Lattes (2016). A maxwell elasto-brittle rheology for sea ice modelling. *The Cryosphere 10*(3), 1339–1359.

[26] Das, N. and P. Chandran (2011). Microbial degradation of petroleum hydrocarbon contaminants: An overview. *Biotechnology Research International*, 1–13.

[27] de Vos, M., M. Barnes, L. Biddle, S. Swart, C.-L. Ramjukadh, and M. Vichi (2021). Evaluating numerical and free-drift forecasts of sea ice drift during a southern ocean research expedition: An operational perspective. *Journal of Operational Oceanography 0*(0), 1–17.

[28] Devis-Morales, A., E. Rodríguez-Rubio, and R. Montoya-Sánchez (2021). Modelling the transport of sediment discharged by colombian rivers to the southern caribbean sea. *Ocean Dynamics 71*, 251 – 277.

[29] Directorate), T. N. P. (2018). Resource report exploration 2018. Online technical report, Norway.

[30] Dupont, F., S. Higginson, R. Bourdallé-Badie, Y. Lu, F. Roy, G. C. Smith, J.-F. Lemieux, G. Garric, and F. Davidson (2015). A high-resolution ocean and sea-ice modelling system for the arctic and north atlantic oceans. *Geoscientific Model Development 8*(5), 1577–1594.

[31] Enhancing oil spill response capability in the Baltic Sea Region (2019). OIL SPILL. https://blogit.utu.fi/oilspill/about-the-project/. [Online; accessed 20 January 2021].

[32] Faksness, L., R. Daae, P. Brandvik, F. Leirvik, and J. Børseth (2010). Oil distribution and bioavailability. field experiment - fex 2009. Summary report, SINTEF.

[33] Faksness, L.-G., P. J. Brandvik, R. L. Daae, F. Leirvik, and J. F. Børseth (2011). Large-scale oil-in-ice experiment in the barents sea: Monitoring of oil in water and metocean interactions. *Marine Pollution Bulletin 62*(5), 976–984.

[34] Fay, J. (1969). The spread of oil slicks on a calm sea. In D. Hoult (Ed.), *Oil on the Sea*, pp. 53–63. Boston: Springer.

[35] Feltham, D. (2005). Granular flow in the marginal ice zone. *Philosophical Transactions of the Royal Society A: Mathematical, Physical and Engineering Sciences 363*(1832), 1677–1700.

[36] Feltham, D. L. (2008). Sea ice rheology. *Annual Review of Fluid Mechanics 40*(1), 91–112.

[37] Fingas, M. (2011). Chapter 23 - an overview of in-situ burning. In M. Fingas (Ed.), *Oil Spill Science and Technology*, pp. 737–903. Boston: Gulf Professional Publishing.

[38] Fingas, M. (2012). Chapter 3 - types of oil and their properties. In *The Basics of Oil Spill Cleanup*, pp. 33 – 42. Taylor & Francis Group.

[39] Fingas, M. (2014). *Introduction to Spill Modeling*, Chapter 10, pp. 285–300. John Wiley & Sons, Ltd.

[40] French-McCay, D., T. Tajalli-Bakhsh, K. Jayko, M. Spaulding, and Z. Li (2018). Validation of oil spill transport and fate modeling in arctic ice. *Arctic Science 4*(1), 71–97.

[41] Furnans, J., B. Hodges, and J. Imberger (2005). Drifter modelling and error assessment in wind driven currents. Online technical report, The University of Texas at Austin.

[42] Furnans, J., B. Hodges, and J. Imberger (2020). State of energy report. Online technical report, Austin, Texas, USA.

[43] Gammelsrød, T., Ø. Leikvin, V. Lien, W. Budgell, H. Loeng, and W. Maslowski (2009). Mass and heat transports in the ne barents sea: Observations and models. *Journal of Marine Systems 75*(1), 56–69.

[44] Gearon, M., D. french McCay, E. Chaite, S. Zamorski, D. Reich, J. Rowe, and D. Schmidt-Etkin (2014). Simap modelling of hypothetical oil spills in the beaufort sea for world wildlife fund (wwf). Summary report, World Wildlife Fundation.

[45] Gjevik, B., E. Nøst, and T. Straume (1994). Model simulations of the tides in the barents sea. *Journal of Geophysical Research: Oceans 99*(C2), 3337–3350.

[46] Haakenstad, H., Ø. Breivik, B. R. Furevik, M. Reistad, P. Bohlinger, and O. J. Aarsnes (2021). Nora3: A non-hydrostatic high-resolutionhindcast for the north sea, the norwegian sea and the barents sea. *Submitted to Journal of Applied Meteorology and Climatology*. Submitted.

[47] Hansen, C., M. Skern-Mauritzen, G. van der Meeren, A. Jähkel, and K. Drinkwater (2016). Set-up of the Nordic and Barents Seas (NoBa) Atlantis Model. http://hdl.handle.net/11250/2408609. [Online; accessed 7 November 2021].

[48] Heorton, H., D. Feltham, and J. Hunt (01 Sep. 2014). The response of the sea ice edge to atmospheric and oceanic jet formation. *Journal of Physical Oceanography 44*(9), 2292 – 2316.

[49] Hole, L., K.-F. Dagestad, J. Röhrs, C. Wettre, V. Kourafalou, Y. Androulidakis, H. Kang, M. Le Hénaff, and O. Garcia-Pineda (2019). The deepwater horizon oil slick: Simulations of river front effects and oil droplet size distribution. *J. Mar. Sci. Eng. 7(*(10), 1–20.

[50] Hole, L., V. de Aguiar, K.-F. Dagestad, V. Kourafalou, Y. Androulidakis, H. Kang, M. Le Hénaff, and A. Calzada (2021). Long term simulations of potential oil spills around cuba. *Marine Pollution Bulletin 167*, 112285.

[51] Hunke, E. C. and J. K. Dukowicz (01 Sep. 1997). An elastic–viscous–plastic model for sea ice dynamics. *Journal of Physical Oceanography 27*(9), 1849 – 1867.

[52] Huserbråten, M., E. Eriksen, H. Gjøsæter, and F. Vikebø ("2019"). Polar cod in jeopardy under the retreating arctic sea ice. *Commun Biol 2 407*.

[53] Incardona, J. P., M. G. Carls, L. Holland, T. L. Linbo, D. H. Baldwin, M. S. Myers, K. A. Peck, M. Tagal, S. D. Rice, and N. L. Scholz (2015). Very low embryonic crude oil exposures cause lasting cardiac defects in salmon and herring. *Nature Scientific reports 5*(13499).

[54] Informatics, R. R. (2012). Modeling of potential oil spill behavior when operating Prirazlomnaya OIFP - Assessment of possible oil spill emergency response. Technical report, Wild World Foundation (WWF).

[55] Johannessen, J., O. Johannessen, E. Svendsen, R. Shuchman, T. Manley, W. Campbell, E. Josberger, S. Sandven, J. Gascard, T. Olaussen, K. Davidson, and J. Van Leer (1987). Mesoscale eddies in the fram strait marginal ice zone during the 1983 and 1984 marginal ice zone experiments. *J. Geophys. Res. 92*(C7), 6754–6772.

[56] Johannessen, O. M., J. A. Johannessen, J. Morison, B. A. Farrelly, and E. A. S. Svendsen (1983). Oceanographic conditions in the marginal ice zone north of svalbard in early

fall 1979 with an emphasis on mesoscale processes. *Journal of Geophysical Research: Oceans 88*(C5), 2755–2769.

[57] Johannessen, O. M., H. Sagen, Ø. Nesse, I. Engelsen, and S. Sanvend (1992). Ambient noise generation by ice-ocean jets, eddies and tidal current in the marginal ice zone. In *European Conference on Underwater Acoustics, Weydert, M. (ed)*, pp. 28–38. Elsevier Applied Science.

[58] Jones, C. E., K.-F. Dagestad, Ø. Breivik, B. Holt, J. Röhrs, K. H. Christensen, M. Espeseth, C. Brekke, and S. Skrunes (2016). Measurement and modeling of oil slick transport. *Journal of Geophysical Research: Oceans 121*(10), 7759–7775.

[59] Kostianoy, A., C. Ambjorn, and D. Soloviev (2008). Seatrack web: A numerical tool to protect the baltic sea marine protected areas. In *2008 IEEE/OES US/EU-Baltic International Symposium*, pp. 1–6.

[60] Kozlov, I., A. Artamonova, G. Manucharyan, and A. Kubryakov (2019). Eddies in the western arctic ocean from spaceborne sar observations over open ocean and marginal ice zones. *Journal of Geophysical Research: Oceans 124*(9), 6601–6616.

[61] Laurel, B., , L. Copeman, P. Iseri, M. Spencer, G. Hutchinson, T. Nordtug, C. Donald, S. Meier, S. Allan, D. Boyd, G. Ylitalo, J. Cameron, B. French, T. Linbo, N. Scholz, and J. Incardona (2019). Embryonic crude oil exposure impairs growth and lipid allocation in a keystone arctic forage fish. *iScience 19*, 1101–1113.

[62] Lemieux, J.-F., C. Beaudoin, F. Dupont, F. Roy, G. C. Smith, A. Shlyaeva, M. Buehner, A. Caya, J. Chen, T. Carrieres, L. Pogson, P. DeRepentigny, A. Plante, P. Pestieau, P. Pellerin, H. Ritchie, G. Garric, and N. Ferry (2016). The regional ice prediction system (rips): verification of forecast sea ice concentration. *Quarterly Journal of the Royal Meteorological Society 142*(695), 632–643.

[63] Lien, V., Y. Gusdal, J. Albretsen, A. Melsom, and F. Vikebø (2013). Evaluation of a nordic seas 4 km numerical ocean model hindcast archive (svim), 1960-2011. *Fisken Og Havet 7*, 1–80.

[64] Liu, Y. and R. Weisberg (2011). Evaluation of trajectory modeling in different dynamic regions using normalized cumulative lagrangian separation. *Journal of Geophysical Research: Oceans 116*(C9), 1–13.

[65] Liu, Y., R. Weisberg, S. Vignudelli, and G. Mitchum (2014). Evaluation of altimetry-derived surface current products using lagrangian drifter trajectories in the eastern gulf of mexico. *Journal of Geophysical Research: Oceans 119*(5), 2827–2842.

[66] Loeng, H. (1991). Features of the physical oceanographic conditions of the barents sea. *Polar Research 10*(1), 5–18.

[67] Lüpkes, C. and V. Gryanik (2015). A stability-dependent parametrization of transfer coefficients for momentum and heat over polar sea ice to be used in climate models. *Journal of Geophysical Research: Atmospheres 120*(2), 552–581.

[68] Marchenko, A., J. Rabault, G. Sutherland, C. O. Collins, P. Wadhams, and M. Chumakov (2017). Field observations and preliminary investigations of a wave event in solid drift ice in the barents sea. In *Proceedings-International Conference on Port and Ocean Engineering under Arctic Conditions*. Port and Ocean Engineering under Arctic Conditions.

[69] Martin, T., M. Tsamados, D. Schroeder, and D. Feltham (2016). The impact of variable sea ice roughness on changes in arctic ocean surface stress: A model study. *Journal of Geophysical Research: Oceans 121*(3), 1931–1952.

[70] Monfils, R. (2005, 05). THE GLOBAL RISK OF MARINE POLLUTION FROM WWII SHIPWRECKS: EXAMPLES FROM THE SEVEN SEAS. *International Oil Spill Conference Proceedings 2005*(1), 1049–1054.

[71] Moreira, A. and M. Santos (2007). Concave hull: A k-nearest neighbours approach for the computation of the region occupied by a set of points. In *GRAPP'07, Barcelona, Spain*, pp. 61–68.

[72] Morell Villalonga, M., M. Espino Infantes, M. Grifoll Colls, and M. Mestres Ridge (2020). Environmental management system for the analysis of oil spill risk using probabilistic simulations. application at tarragona monobuoy. *Journal of Marine Science and Engineering 8*(4).

[73] Muench, R. and J. Schumacher (1985). On the bering sea ice edge front. *Journal of Geophysical Research: Oceans 90*(C2), 3185–3197.

[74] Nahrgang, J., P. Dubourg, M. Frantzen, D. Storch, F. Dahlke, and J. P. Meador (2016). Early life stages of an arctic keystone species (boreogadus saida) show high sensitivity to a water-soluble fraction of crude oil. *Environmental Pollution 218*, 605 – 614.

[75] Nordam, T., C. Beegle-Krause, J. Skancke, R. Nepstad, and M. Reed (2019). Improving oil spill trajectory modelling in the arctic. *Marine Pollution Bulletin 140*, 65 – 74.

[76] Nordam, T., D. Dunnebier, C. Beegle-Krause, M. Reed, and D. Slagstad (2017). Impact of climate change and seasonal trends on the fate of arctic oil spills. *Ambio 46*, 442–452.

[77] Onarheim, I. and M. Årthun (2017). Toward an ice-free barents sea. *Geophysical Research Letters 44*(16), 8387–8395.

[78] OSPAR Commission (2021). Offshore Installations — Webpage. OSPAR Commission. https://www.ospar.org/work-areas/oic/installations. [Online; accessed 28 May 2021].

[79] Pereiro, D., C. Souto, and J. Gago (2018). Calibration of a marine floating litter transport model. *Journal of Operational Oceanography 11*(2), 125–133.

[80] Petty, A. A., M. C. Tsamados, and N. T. Kurtz (2017). Atmospheric form drag coefficients over arctic sea ice using remotely sensed ice topography data, spring 2009–2015. *Journal of Geophysical Research: Earth Surface 122*(8), 1472–1490.

[81] Platov, G. and E. Golubeva (2020, dec). Characteristics of mesoscale eddies of arctic marginal seas: results of numerical modeling. *IOP Conference Series: Earth and Environmental Science 611*, 012009.

[82] Rabatel, M., P. Rampal, A. Carrassi, L. Bertino, and C. K. R. T. Jones (2018). Impact of rheology on probabilistic forecasts of sea ice trajectories: application for search and rescue operations in the arctic. *The Cryosphere 12*(3), 935–953.

[83] Rabault, J., G. Sutherland, O. Gundersen, and A. Jensen (2017). Measurements of wave damping by a grease ice slick in svalbard using off-the-shelf sensors and open-source electronics. *Journal of Glaciology 63*(238), 372–381.

[84] Rabault, J., G. Sutherland, O. Gundersen, and A. Jensen (2019). An open source, versatile, affordable waves in ice instrument for remote sensing in the polar regions. *arXiv preprint arXiv:1901.02410*.

[85] Rampal, P., S. Bouillon, E. Ólason, and M. Morlighem (2016). nextsim: a new lagrangian sea ice model. *The Cryosphere 10*(3), 1055–1073.

[86] Reed, M. and O. Aamo (1994). Real time oil spill forecasting during an experimental oil spill in the arctic ice. *Spill Science & Technology Bulletin 1*(1), 69 – 77.

[87] Reed, M., Øistein Johansen, P. J. Brandvik, P. Daling, A. Lewis, R. Fiocco, D. Mackay, and R. Prentki (1999). Oil spill modeling towards the close of the 20th century: Overview of the state of the art. *Spill Science & Technology Bulletin 5*(1), 3 – 16.

[88] Röhrs, J., K.-F. Dagestad, H. Asbjørnsen, T. Nordam, J. Skancke, C. E. Jones, and C. Brekke (2018). The effect of vertical mixing on the horizontal drift of oil spills. *Ocean Science 14*(6), 1581–1601.

[89] Romagnoni, G., K. Ø. Kvile, K.-F. Dagestad, A. Eikeset, T. Kristiansen, N. Stenseth, and Ø. Langangen (2020). Influence of larval transport and temperature on recruitment dynamics of north sea cod (gadus morhua) across spatial scales of observation. *Fisheries Oceanography 29*(4), 324–339.

[90] Sakov, P., F. Counillon, L. Bertino, K. A. Lisåter, P. R. Oke, and A. Korablev (2012). Topaz4: an ocean-sea ice data assimilation system for the north atlantic and arctic. *Ocean Sci. 8*, 633 – 656.

[91] Schrum, C., I. Alekseeva, and M. St. John (2006). Development of a coupled physical–biological ecosystem model ecosmo: Part i: Model description and validation for the north sea. *Journal of Marine Systems 61*(1), 79–99.

[92] Serreze, M., M. Holland, and J. Stroeve (2007). Perspectives on the arctic's shrinking sea-ice cover. *Science 315*(5818), 1533–1536.

[93] Simecek-Beatty, D. (2011). Chapter 11 - oil spill trajectory forecasting uncertainty and emergency response. In M. Fingas (Ed.), *Oil Spill Science and Technology*, pp. 275 – 299. Boston: Gulf Professional Publishing.

[94] Simonsen, M., B. Hackett, L. Bertino, L. Rø, G. Waagbø, M. Drivdal, and G. Sutherland (2019). *Product User Manual For Arctic Ocean Physical and BIO Analysis and Forecasting Products*. Copernicus Marine Environment Monitoring Service.

[95] Smith, G., F. Roy, M. Reszka, D. Surcel Colan, Z. He, D. Deacu, J.-M. Belanger, S. Skachko, Y. Liu, F. Dupont, J.-F. Lemieux, C. Beaudoin, B. Tranchant, M. Drévillon, G. Garric, C.-E. Testut, J.-M. Lellouche, P. Pellerin, H. Ritchie, Y. Lu, F. Davidson, M. Buehner, A. Caya, and M. Lajoie (2016). Sea ice forecast verification in the canadian global ice ocean prediction system. *Quarterly Journal of the Royal Meteorological Society 142*(695), 659–671.

[96] Snow, N. and I. D. C. (NSIDC) (2017). Sea ice index, version 3. monthly sea ice concentration images, north. https://doi.org/10.7265/N5K072F8. [Online; accessed 13 July 2020].

[97] Solbrekke, I. M., A. Sorteberg, and H. Haakenstad (2021). Norwegian hindcast archive (nora3) – a validation of offshore wind resources in the north sea and norwegian sea. *Wind Energy Science Discussions 2021*, 1–31.

[98] Sørstrøm, S., P. Brandvik, I. Buist, P. Daling, D. Dickins, L. Faksness, S. Potter, J. Fritt-Rasmussen, and I. Singsaas (2010). Joint industry program on oil contingency for arctic and ice-covered waters. Summary report, SINTEF.

[99] Sutherland, G. and J. Rabault (2016). Observations of wave dispersion and attenuation in landfast ice. *Journal of Geophysical Research: Oceans 121*(3), 1984–1997.

[100] Tamtare, T., D. Dumont, and C. Chavanne (2021). The stokes drift in ocean surface drift prediction. *Journal of Operational Oceanography 0*(0), 1–13.

[101] Taylor, P., M. Cramer, R. Cox, and R. Santner (2018). From net environmental benefit analysis to spill impact mitigation assessment sima. Paper presented at the SPE International Conference and Exhibition on Health, Safety, Security, Environment, and Social Responsibility, Abu Dhabi. OnePetro.

[102] The International Tanker Owners Pollution Federation (2020). Oil Tanker Spill Statistics 2019, special edition: 50 years of data, 1970 - 2019. https://www.itopf.org/fileadmin/data/Documents/Company_Lit/Oil_Spill_Stats_brochure_2020_for_web.pdf. [Online; accessed 24 October 2020].

[103] Thomson, R. E. and W. J. Emery (2014). Chapter 3 - statistical methods and error handling. In R. Thomson and W. Emery (Eds.), *Data Analysis Methods in Physical Oceanography (Third Edition)* (Third Edition ed.)., pp. 219 – 311. Boston: Elsevier.

[104] Tkalich, P. and E. S. Chan (2002). Vertical mixing of oil droplets by breaking waves. *Marine Pollution Bulletin 44*(11), 1219–1229.

[105] Transportation Research Board and National Research Council (2003). *Oil in the Sea III: Inputs, Fates, and Effects*. Washington, DC: The National Academies Press.

[106] Tsamados, M., D. L. Feltham, D. Schroeder, D. Flocco, S. L. Farrell, N. Kurtz, S. W. Laxon, and S. Bacon (01 May. 2014). Impact of variable atmospheric and oceanic form drag on simulations of arctic sea ice. *Journal of Physical Oceanography 44*(5), 1329 – 1353.

[107] Tuomi, L., O. Vähä-Piikkiö, P. Alenius, J.-V. Björkqvist, and K. Kahma (2018). Surface stokes drift in the baltic sea based on modelled wave spectra. *Ocean Dynamics 68*, 17–33.

[108] van Sebille, E., S. M. Griffies, R. Abernathey, T. P. Adams, P. Berloff, A. Biastoch, B. Blanke, E. P. Chassignet, Y. Cheng, C. J. Cotter, E. Deleersnijder, K. Döös, H. F. Drake, S. Drijfhout, S. F. Gary, A. W. Heemink, J. Kjellsson, I. M. Koszalka, M. Lange, C. Lique, G. A. MacGilchrist, R. Marsh, C. G. Mayorga Adame, R. McAdam, F. Nencioli, C. B. Paris, M. D. Piggott, J. A. Polton, S. Rühs, S. H. Shah, M. D. Thomas, J. Wang, P. J. Wolfram, L. Zanna, and J. D. Zika (2018). Lagrangian ocean analysis: Fundamentals and practices. *Ocean Modelling 121*, 49 – 75.

[109] Vatne, E. (2018). Sysselsetting i petroleumsvirksomhet 2017omfang og lokalisering av ansatte i oljeselskap og den spesialiserte leverandørindustrien. Online technical report, Bergen, Norway.

[110] Venkatesh, S., H. El-Tahan, G. Comfort, and R. Abdelnour (1990). Modelling the behaviour of oil spills in ice-infested waters. *Atmos. Ocean 28*(3), 303–329.

[111] Visser, A. W. (1997). Using random walk models to simulate the vertical distribution of particles in a turbulent water column. *Mar. Ecol. Prog. Ser. 158*, 275–281.

[112] Wadhams, P. and N. Davis (2000). Further evidence of ice thinning in the arctic ocean. *Geophysical Research Letters 27*(24), 3973–3975.

[113] Wang, Q., N. Koldunov, S. Danilov, D. Sidorenko, C. Wekerle, P. Scholz, I. Bashmachnikov, and T. Jung (2020). Eddy kinetic energy in the arctic ocean from a global simulation with a 1-km arctic. *Geophysical Research Letters 47*(14), e2020GL088550. e2020GL088550 10.1029/2020GL088550.

[114] Wassmann, P., M. Reigstad, T. Haug, B. Rudels, M. Carroll, H. Hop, G. Gabrielsen, S. Falk-Petersen, S. Denisenko, E. Arashkevich, D. Slagstad, and O. Pavlova (2006). Food webs and carbon flux in the barents sea. *Progress in Oceanography 71*(2), 232–287. Structure and function of contemporary food webs on Arctic shelves: a pan-Arctic comparison.

[115] Wekerle, C., T. Hattermann, Q. Wang, L. Crews, W.-J. von Appen, and S. Danilov (2020). Properties and dynamics of mesoscale eddies in fram strait from a comparison between two high-resolution ocean–sea ice models. *Ocean Science 16*(5), 1225–1246.

[116] Wilkinson, J., C. Beegle-Krause, K. Evers, N. Hughes, A. Lewis, M. Reed, and P. Wadhams (2017). Oil spill response capabilities and technologies for ice-covered arctic marine waters: A review of recent developments and established practices. *Ambio 93*, 423–441.

[117] Willmott, C. (1981). On the validation of models. *Physical Geography 2*(2), 184–194.

[118] Wong, A., K. Robert, C. Thierry, and the Argo Data Management Team (2020). Argo quality control manual for ctd and trajectory data. Report, USA, FRANCE.

[119] Xie, J. and L. Bertino (2021). *Quality Information Document - Arctic Physical Multi Year Product ARCTIC_MULTIYEAR_PHY_002_003*. Copernicus Marine Environment Monitoring Service.

[120] Yapa, P. and L. Dasanayaka (2006). State-of-the-art review of modelling oil transport and spreading in ice covered waters. In *Arctic and Marine Oilspill Program (AMOP)*, Volume 893.

[121] Zhang, X., L. Cheng, F. Zhang, J. Wu, S. Li, J. Liu, S. Chu, N. Xia, K. Min, X. Zuo, and M. Li (2020). Evaluation of multi-source forcing datasets for drift trajectory prediction using lagrangian models in the south china sea. *Applied Ocean Research 104*, 102395.

Appendix A

Spill surface area estimation

The surface area covered by the simulated oil slicks in the hypothetical oil accident in the Pechora Sea (see 3.0.3) was estimated by using the concave-hull method. The first step is to define the polygon that encircles the cloud of particles, or different patches of particles, by using a computational geometry algorithm. Many approaches (*e.g.* K-nearest, DBSCAN, Graham Scan and Jarvis March) can be used, but in this work the so-called alpha shape was applied.

The alpha shape can be constructed by conducting Delaunay triangulation (or tesselation) over a set of points S, which here are represented by the virtual particles released in OpenDrift. Triangles are formed over the three nearest points and for each triangle a sorrounding *circumcirle* is created. The circumcircle is the smallest circle which the triangle can be inscribed. The radius of such a circumcircle is called *circumradius*. A selection parameter α (alpha value) is defined and each circumradius is then compared to the alpha value. If the circumradius > alpha value, the corresponding triangle is removed. Otherwise, it is merged in the alpha shape envelope. The process is iterated over the whole set of triangles to obtain the concave-hull polygon.

A thorough description can be found in (71) and a Jupiter notebook tutorial created by me to exemplify the process is available at https://github.com/vic1309/concave_hull_area/blob/master/surface_area.ipynb.